0026-895X/10/7704-704–713$20.00
MOLECULAR PHARMACOLOGY
Copyright © 2010 The American Society for Pharmacology and Experimental Therapeutics
Mol Pharmacol 77:704–713, 2010

Vol. 77, No. 4
61481/3574034
Printed in U.S.A.

Sphingosine 1-Phosphate (S1P) Regulates Vascular Contraction via $S1P_3$ Receptor: Investigation Based on a New $S1P_3$ Receptor Antagonist[S]

Akira Murakami, Hiroshi Takasugi, Shinya Ohnuma, Yuuki Koide, Atsuko Sakurai, Satoshi Takeda, Takeshi Hasegawa, Jun Sasamori, Takashi Konno, Kenji Hayashi, Yoshiaki Watanabe, Koji Mori, Yoshimichi Sato, Atsuo Takahashi, Naoki Mochizuki, and Nobuyuki Takakura

Tokyo Research Laboratories, Drug Research Department (A.M., H.T., S.O., Y.K., Y.S.), and Fukushima Research Laboratories, Drug Research Department (T.H., J.S., T.K., K.H., Y.W., K.M., A.T.), TOA EIYO Ltd., Fukushima, Japan; Department of Emergency Medicine, Jikei University School of Medicine, Tokyo, Japan (S.T.); Department of Structural Analysis, National Cardiovascular Center Research Institute, Osaka, Japan (A.S., N.M.); and Department of Signal Transduction, Research Institute for Microbial Diseases, Osaka University, Osaka, Japan (N.T.)

Received October 13, 2009; accepted January 19, 2010

ABSTRACT

Sphingosine 1-phosphate (S1P) induces diverse biological responses in various tissues by activating specific G protein-coupled receptors ($S1P_1$–$S1P_5$ receptors). The biological signaling regulated by $S1P_3$ receptor has not been fully elucidated because of the lack of an $S1P_3$ receptor-specific antagonist or agonist. We developed a novel $S1P_3$ receptor antagonist, 1-(4-chlorophenylhydrazono)-1-(4-chlorophenylamino)-3,3-dimethyl-2-butanone (TY-52156), and show here that the S1P-induced decrease in coronary flow (CF) is mediated by the $S1P_3$ receptor. In functional studies, TY-52156 showed submicromolar potency and a high degree of selectivity for $S1P_3$ receptor. TY-52156, but not an $S1P_1$ receptor antagonist [(*R*)-phosphoric acid mono-[2-amino-2-(3-octyl-phenylcarbamoyl)-ethyl] ester; VPC23019] or $S1P_2$ receptor antagonist [1-[1,3-dimethyl-4-(2-methylethyl)-1*H*-pyrazolo[3,4-*b*]pyridin-6-yl]-4-(3,5-dichloro-4-pyridinyl)-semicarbazide; JTE013], inhibited the decrease in CF induced by S1P in isolated perfused rat hearts. We further investigated the effect of TY-52156 on both the S1P-induced increase in intracellular calcium ($[Ca^{2+}]_i$) and Rho activation that are responsible for the contraction of human coronary artery smooth muscle cells. TY-52156 inhibited both the S1P-induced increase in $[Ca^{2+}]_i$ and Rho activation. In contrast, VPC23019 and JTE013 inhibited only the increase in $[Ca^{2+}]_i$ and Rho activation, respectively. We further confirmed that TY-52156 inhibited FTY-720-induced $S1P_3$ receptor-mediated bradycardia in vivo. These results clearly show that TY-52156 is both sensitive and useful as an $S1P_3$ receptor-specific antagonist and reveal that S1P induces vasoconstriction by directly activating $S1P_3$ receptor and through a subsequent increase in $[Ca^{2+}]_i$ and Rho activation in vascular smooth muscle cells.

Sphingosine 1-phosphate (S1P) is a bioactive lysophospholipid mediator that is mainly released from activated platelets and induces many biological responses, including angiogenesis, vascular development, and cardiovascular function (Siess, 2002; Yatomi, 2006; Takuwa et al., 2008). A wide variety of biological cellular responses to S1P have been ascribed to the presence of five S1P receptors, $S1P_1$ to $S1P_5$ receptors, that belong to the family of G protein-coupled receptors (GPCRs). Furthermore, a variation of heterotrimeric G protein downstream of S1P receptors accounts for the diversity of cellular responses to S1P (Rosen et al., 2009). In addition to the coupling of S1P receptors and G proteins, the expression of the combi-

This work was supported by Research on Health Science Focusing on Drug Innovation from the Japan Health Sciences Foundation [Grant KHC1016].

Article, publication date, and citation information can be found at http://molpharm.aspetjournals.org.

doi:10.1124/mol.109.061481.

[S] The online version of this article (available at http://molpharm.aspetjournals.org) contains supplemental material.

ABBREVIATIONS: S1P, sphingosine 1-phosphate; GPCR, G protein-coupled receptor; TY-52156, 1-(4-chlorophenylhydrazono)-1-(4-chlorophenylamino)-3,3-dimethyl-2-butanone; MAPK, mitogen-activated protein kinase; CF, coronary flow; HUVEC, human umbilical vein endothelial cell; HCASMC, human coronary artery smooth muscle cell; SBP, systemic blood pressure; HR, heart rate; MBP, mean blood pressure; JTE013, 1-[1,3-dimethyl-4-(2-methylethyl)-1*H*-pyrazolo[3,4-*b*]pyridin-6-yl]-4-(3,5-dichloro-4-pyridinyl)-semicarbazide; VPC23019, (*R*)-phosphoric acid mono-[2-amino-2-(3-octyl-phenylcarbamoyl)-ethyl] ester; SD, Sprague-Dawley; Ik_{Ach}, cardiac G protein-gated potassium channel; Eu-GTP, europium-GTP; LC/MS/MS, liquid chromatography/tandem mass spectrometry; U46619, 9,11-dideoxy-9α,11α-methanoepoxy prostaglandin $F_2\alpha$; FTY-720, fingolimod; Y-27632, (*R*)-(+)-*trans*-4-(1-aminoethyl)-*N*-(4-pyridyl)cyclohexanecarboxamide dihydrochloride monohydrate; SEW2871, 5-[4-phenyl-5-(trifluoromethyl)-2-thienyl]-3-[3-(trifluoromethyl)phenyl]-1,2,4-oxadiazole.

nation of S1P receptors determines multiple cellular responses. To identify the signaling that is specific for each receptor, S1P receptor antagonists have been developed and have contributed to our understanding of S1P-mediated signaling (Huwiler and Pfeilschifter, 2008).

$S1P_1$ to $S1P_5$ receptors couple to different G proteins upon binding to S1P. Whereas $S1P_1$, $S1P_4$, and $S1P_5$ receptors mainly couple to G_i, $S1P_2$ and $S1P_3$ receptors couple to G_i, G_q, and $G_{12/13}$ (Rosen et al., 2009). The signal that converges from G_i-coupled S1P receptors inhibits the activation of adenylate cyclase and induces the activation of p44/p42 mitogen-activated protein kinase (MAPK). Although the $S1P_1$ receptor slightly increases intracellular calcium ($[Ca^{2+}]_i$) through $G\beta\gamma$, $S1P_2$ and $S1P_3$ receptors mainly increase $[Ca^{2+}]_i$ through the activation of phospholipase Cβ from G_q (Watterson et al., 2005). The deletion of $S1P_3$ but not $S1P_2$ receptor in mouse embryonic fibroblasts led to the marked inhibition of S1P-induced phospholipase C activation, which suggests that $S1P_3$ receptor plays an important role in the S1P-induced increase in $[Ca^{2+}]_i$ (Ishii et al., 2002).

$S1P_2$ and $S1P_3$ receptors also couple to $G_{12/13}$ protein to activate a small GTPase, Rho, which is involved in the regulation of actin-cytoskeleton (Ryu et al., 2002; Sugimoto et al., 2003). Rho kinase is activated by Rho through the $G_{12/13}$-Rho guanine nucleotide exchange factor family. S1P-induced Rho activation has been shown to be significantly reduced in $S1P_2$ but not $S1P_3$ receptor-null mouse embryonic fibroblasts (Ishii et al., 2002). Meanwhile, an association between $S1P_3$ receptor and Rho activation has been reported in cells expressing $S1P_3$ receptor (Sugimoto et al., 2003). An S1P-induced contraction of vascular smooth muscle cells has been ascribed to an increase in $[Ca^{2+}]_i$ and Rho activation (Ohmori et al., 2003; Watterson et al., 2005). S1P-induced vasoconstriction is significantly inhibited in cerebral arteries isolated from $S1P_3$ receptor-null mice but not in those from $S1P_2$ receptor-null mice (Salomone et al., 2008). In addition, Y-27632, a selective Rho kinase inhibitor, inhibits S1P-induced vasoconstriction in canine cerebral arteries (Tosaka et al., 2001), indicating that $S1P_3$ receptor plays an indispensable role in S1P-induced vasoconstriction mediated by Rho-Rho kinase signaling. Although S1P decreases coronary flow (CF) in isolated perfused canine heart, the receptor subtype that is responsible for the S1P-induced reduction of CF has not yet been fully identified. To distinguish $S1P_3$ receptor-dependent signal from $S1P_2$ receptor-dependent signal, an $S1P_3$ receptor-specific antagonist has been needed.

We have developed an $S1P_3$ receptor antagonist, TY-52156. By confirming that TY-52156 has a selective antagonistic effect toward $S1P_3$ receptor, we can delineate the role of $S1P_3$ receptor-specific signaling in vascular contraction. Moreover, the effectiveness of TY-52156 in vivo was bolstered by evidence that $S1P_3$ receptor-dependent bradycardia was suppressed by the oral administration of TY-52156.

Materials and Methods

Materials

TY-52156 was synthesized in our laboratories. Materials were purchased from the following suppliers: S1P was from BIOMOL Research Laboratories (Plymouth Meeting, PA); SEW2871, FTY-720 and FTY-720-(*S*)-Phosphate were from Cayman Chemical (Ann Arbor, MI); VPC23019 was from Avanti Polar Lipids, Inc. (Alabaster, AL); JTE013 was from Tocris Bioscience (Southampton, UK); U46619 was from Calbiochem (Darmstadt, Germany); HuMedia-EG2 and HuMedia-SG2 were from Kurabo (Osaka, Japan); and membranes containing human $S1P_1$, $S1P_2$, $S1P_3$, or $S1P_5$ receptors were from Millipore (Billerica, MA).

Synthesis of TY-52156

5,5-Dimethyl-2,4-dihexanone (1). Diisopropyl ether (3 liters) was placed in a 5-liter three-neck round-bottomed flask and stirred mechanically. Potassium *tert*-butoxide (324 g, 2.25 mol, 1.5 eq) was suspended in the diisopropyl ether at 0°C. Pinacolone (150 g, 1.50 mol, 1.0 eq) in ethyl acetate (440 ml, 4.50 mol, 3.0 eq) was slowly added drop-wise so that the temperature would remain below 10°C under ice-bath cooling. The reaction mixture was then stirred for 20 h at ambient temperature. Water (1 liter) was added slowly so that the temperature would remain below 10°C under ice-bath cooling. The separated organic layer was extracted with 1 N sodium hydroxide (150 ml). The basic aqueous layer was carefully acidified with 6 N HCl (750 ml, 2.0 equivalents of base) at 0°C and then extracted twice with petroleum ether (750 ml). The combined organic layer was washed with water (475 ml) and saturated brine (475 ml), dried over anhydrous sodium sulfate, filtered, and evaporated at 200 mm Hg and ambient temperature. The remaining liquid was distilled under reduced pressure with heating up to 80°C. The compound (**1**) was obtained as a colorless oil (126 g, 0.89 mol, 59%); ^{1}H NMR (300 MHz, $CDCl_3$) δ: 1.17 (s, 9 H), 2.08 (s, 3 H), 5.61 (s, 1 H); boiling point: 62 to 69°C (20 mm Hg).

3-Chloro-5,5-dimethyl-2,4-dihexanone (2). 5,5-Dimethyl-2,4-dihexanone (**1**) (35.4 g, 249 mmol, 1.0 eq) was dissolved in chloroform (700 ml) and stirred mechanically. Sulfuryl chloride (260 ml, 324 mmol, 1.3 eq) in chloroform (130 ml) was slowly added drop-wise so that the temperature would remain below 5°C under ice-bath cooling. The reaction mixture was then stirred for 2 h at 25°C and then quenched with water (500 ml) at 0°C. The separated organic layer was washed three times with water (500 ml), dried over anhydrous sodium sulfate, filtered, and evaporated. The residue was purified by distillation under reduced pressure with heating to 70°C. The title compound (**2**) was obtained as a yellow oil (41.5 g, 235 mmol, 94%); ^{1}H NMR (300 MHz, $CDCl_3$) δ: 1.23 (s, 9 H), 2.38 (s, 3 H), 5.09 (s, 1 H); boiling point: 67 to 69°C (1.5 mm Hg).

[1-Chloro-1-(4-chlorophenylhydrazono)]-3,3-dimethyl-2-butanone (3). 4-Chloroaniline (29 g, 226 mmol, 1.0 eq) was added to 6 N hydrochloric acid (158 ml, 951 mmol, 4.2 eq) and water (68 ml) and stirred for 15 min at 0°C. Sodium nitrite (17 g, 249 mmol, 1.1 eq) in water (90 ml) was slowly added drop-wise so that the temperature would remain below 5°C under ice-bath cooling. The reaction mixture was stirred for 1 h at 0°C to prepare a solution of diazonium salt. 3-Chloro-5,5-dimethyl-2,4-dihexanone (**2**) (40 g, 226 mmol, 1.0 eq) was dissolved in pyridine (158 ml) and water (158 ml) at 0°C. The previously prepared diazonium salt solution was slowly added drop-wise so that the temperature would remain below 10°C, and the resulting mixture was then vigorously stirred for 2 h with warming from 0 to 25°C. The reaction mixture was extracted with ethyl acetate (452 ml), washed twice with 2 N HCl (1 liter) and saturated brine (452 ml), dried over anhydrous sodium sulfate, filtered, and evaporated. The resulting crude product was diluted with methanol (226 ml, 1 M solution), refluxed for 1 h and then cooled to 0°C. The precipitated crude crystals were collected by filtration, washed with petroleum ether, and dried under reduced pressure to give the title compound (**3**) as a yellow solid (24 g, 89 mmol, 39%); ^{1}H NMR (300 MHz, $CDCl_3$) δ: 1.43 (s, 9H), 7.12 (d, J = 8.7 Hz, 2H), 7.33 (d, J = 8.7 Hz, 2H), 8.34 (s, 1H); melting point: 129 to 131°C.

TY-52156. [1-Chloro-1-(4-chlorophenylhydrazono)]-3,3-dimethyl-2-butanone (**3**) (22.4 g, 82.1 mmol, 1.0 eq) and 4-chloroaniline (11.5 g, 90.4 mmol, 1.1 eq) were dissolved in ethanol (274 ml), and triethylamine (13.7 ml, 98.6 mmol, 1.2 eq) was then added at 0°C. The

resulting mixture was stirred for 3 h at ambient temperature. The reaction mixture was evaporated, quenched with water (82 ml), and diluted with ethyl acetate (165 ml). The organic layer was washed with water (165 ml) and saturated brine (165 ml), dried over anhydrous sodium sulfate, filtered, and evaporated. The resulting crude crystals were washed with a solvent mixture of hexane-ethyl acetate (20:1) and dried under reduced pressure to obtain TY-52156 as a yellow powder (24.8 g, 68.1 mmol, 83%); ^{1}H NMR (300 MHz, $CDCl_3$) δ: 1.48 (s, 9H), 6.55 (d, J = 8.4 Hz, 2H), 6.76 (s, 1H), 6.98 (d, J = 8.8 Hz, 2H), 7.19–7.26 (m, 5H); electrospray ionization-mass spectrometry m/z = 362 $(M\text{-}H)^-$; melting point: 90 to 91°C.

Cell Culture

Chinese hamster ovary K1 cells that stably expressed human $S1P_1$ ($S1P_1$-CHO), $S1P_2$ ($S1P_2$-CHO), or $S1P_3$ ($S1P_3$-CHO) receptors were maintained as described previously (Koide et al., 2007). A human recombinant $S1P_4$ receptor-expressing cell line ($S1P_4$-Chem) was purchased from Millipore. Human umbilical vein endothelial cells (HUVECs) purchased from DS Pharma Biomedical (Osaka, Japan) were cultured on collagen-coated dishes in HuMedia-EG2. Human coronary artery smooth muscle cells (HCASMCs) purchased from Kurabo were cultured in HuMedia-SG2.

Measurement of the Intracellular Calcium Concentration

$[Ca^{2+}]_i$ in $S1P_1$-, $S1P_2$-, $S1P_3$-CHO, and $S1P_4$-Chem was measured using the calcium-sensitive dye Fura-2 acetoxymethyl ester, as described previously (Koide et al., 2007). The fluorescence (excitation at 340 and 380 nm, emission at 510 nm) was measured with a FLEXStation II (Molecular Devices, Sunnyvale, CA). The ratio of the fluorescence intensity at two wavelengths (FR340/380) was calculated. The K_i value for TY-52156 was estimated from Ca^{2+} responses as described previously (Ohta et al., 2003).

[^{3}H]S1P Binding Assay

A [^{3}H]S1P binding assay was performed as described by Lim et al. (2003) with minor modifications. The cell membrane (60 μg/ml) was incubated with binding buffer containing [^{3}H]S1P (1 nM, approximately 40,000 dpm/well) and vehicle or each concentration of TY-52156 (micromolar) for 30 min at 25°C. Radioactivity was measured by a liquid scintillation counter after the addition of scintillation cocktail solution. Nonspecific binding was defined as the amount of radioactivity bound to the cells in the presence of unlabeled S1P (3.0 μM). Specific binding was calculated by subtracting nonspecific binding from total binding.

GTP Binding Assay

Europium-GTP (Eu-GTP) binding was determined using a DELFIA GTP Binding Assay Kit (PerkinElmer Life and Analytical Sciences, Turku, Finland). Samples were incubated in AcroWell filter plates (PALL, Ann Arbor, MI) for 60 ($S1P_1$ and $S1P_5$) or 90 min ($S1P_2$ and $S1P_3$) at 30°C. The reaction was started by adding membranes (48 μg/ml) containing human $S1P_1$, $S1P_2$, $S1P_3$, or $S1P_5$ receptors to the assay buffer (20 mM HEPES, pH 7.4, 5 mM $MgCl_2$, 100 mM NaCl, 1.2 mg/ml saponin, 10 μM GDP, and 10 nM Eu-GTP at 30°C) including S1P (0.1 μM) and vehicle or the desired concentration (micromolar) of the test drug (TY-52156 or VPC23019). The reaction was terminated by rapid filtration, and the filter was washed five times with 200 μl of ice-cold washing solution in a vacuum manifold. The plate was measured by time-resolved fluorescence (340 nm excitation/615 nm emission) using EnVision (PerkinElmer Life and Analytical Sciences).

Western Blot Analysis for p44/p42 MAPK

$S1P_1$-, $S1P_2$-, and $S1P_3$-CHO (2.0×10^5 cells) were plated on six-well plates and cultured with Nutrient Mixture F-12 Ham (Sigma-Aldrich, St. Louis, MO) containing 1% fetal bovine serum for 4 h before the experiments. The cells were treated with vehicle, TY-52156 (10 μM), VPC23019 (10 μM), or JTE013 (1.0 μM) for 10 min and then with vehicle or S1P (0.1 μM) for 5 min at 37°C. The cells were lysed in CelLytic M containing Protease Inhibitor Cocktails and Phosphatase Inhibitor Cocktails (Sigma-Aldrich) for 10 min at 4°C. The lysate was centrifuged at 13,000g for 15 min at 4°C, and supernatant was transferred to a fresh tube. The protein concentration was determined using the Bradford method. Equal amounts of proteins were resuspended in 4× sample buffer (Wako Pure Chemicals, Tokyo, Japan), boiled for 5 min, and separated by 10% SDS-polyacrylamide gel electrophoresis. After being transferred to a polyvinylidene difluoride membrane, the membranes were blocked in Block Ace (DS Pharma Biomedical, Osaka, Japan) and immunoblotted with antibodies of phospho-p44/p42 MAPK or p44/p42 MAPK (1:1000; Cell Signaling Technology, Danvers, MA). The signals were visualized by an Amplified Alkaline Phosphatase Goat Anti-Rabbit Immuno-Blot Assay Kit (Bio-Rad Laboratories, Hercules, CA) according to the manufacturer's instructions. Quantitative analyses of immunoblots were performed using Quantity One version 4.2.2 software (Bio-Rad Laboratories). The relative percentage compared with the vehicle was calculated and expressed as the mean ± S.E.M.

Measurement of Coronary Flow

All animal experiments were reviewed and approved by the Experimental Animal Committee in our laboratories. Male Sprague-Dawley (SD) rats (300–350 g; Nihon Bunko, Tokyo, Japan) were anesthetized by the injection of pentobarbital (50 mg/kg i.p.). After thoracotomy, their hearts were rapidly excised and perfused at 37°C in a Langendorff manner with Krebs-Henseleit bicarbonate buffer (constant perfusion pressure of 70 ± 5 mm Hg) of the following composition: 118 mM NaCl, 4.7 mM KCl, 1.2 mM KH_2PO_4, 1.2 mM $MgSO_4$; 2.5 mM $CaCl_2$, 24.9 mM $NaHCO_3$, 0.027 mM EDTA/2Na^+, 0.057 mM ascorbic acid, and 11.1 mM glucose, pH 7.4, at 37°C, bubbled with 95% O_2/5% CO_2 (pO_2 > 550 mm Hg). A modified water-filled latex balloon (Technical Service Corporation, Louisville, KY) was inserted into the left ventricle via the left atrium with a pressure transducer (Ohmeda PPD, Liberty Corner, NJ) connected to an amplifier (Nihon Kohden). Left ventricular end-diastolic pressure was adjusted to approximately 5 to 10 mm Hg. To measure CF, a Cannulating-Type Flow Probe (Nihon Kohden) connected to an electromagnetic blood flowmeter (Nihon Kohden) was inserted to the perfusion line that was connected to the heart. After a 15-min period for equilibration, vehicle, TY-52156 (0.1 μM), VPC23019 (0.1 μM), or JTE013 (0.1 μM) was infused for 10 min by an infusion pump (Harvard Apparatus Inc., Holliston, MA) through a drug-infusion line connected to the main perfusion line at a flow rate of 1/100 the CF rate. After drug treatment, vehicle or the indicated concentration of S1P (micromolar) or U46619 (0.1 μM) was added to the same line. CF was measured before and 10 min after the infusion of S1P or U46619. The relative percentage compared with the vehicle was calculated from the CF rate.

Contractile Response in Cerebral Arteries

Beagle dogs (Oriental Yeast, Tokyo, Japan) were anesthetized by the injection of pentobarbital (30 mg/kg i.p.). The cerebral arteries were rapidly excised and mounted in organ chambers containing Krebs buffer of the following composition: 118.0 mM NaCl, 4.7 mM KCl, 2.5 mM $CaCl_2$, 1.2 mM KH_2PO_4, 1.2 mM $MgSO_4$, 25.0 mM $NaHCO_3$, and 11.0 mM glucose, pH 7.2, at 37°C, bubbled with 95% O_2/5% CO_2. After equilibration, cerebral arteries were exposed to 60 mM KCl until the contractile responses were stabilized. After washout and recovery, contractile responses to S1P were measured every 10 min after the addition of the indicated concentration of S1P (micromolar). In another experiment, the cerebral arteries were contracted by S1P (5.0 μM), and then an increasing amount of vehicle or TY-52156 (up to 10 μM) was applied to the organ chambers. Relaxation responses were measured every 10 min after the addition of the indicated concentration of vehicle or TY-52156 (micromolar). The

degree of contraction compared with vehicle was calculated with Prism (ver. 4; GraphPad Software Inc., San Diego, CA) and expressed as the percentage of contraction compared with that induced by S1P.

Immunoprecipitation and Western Blot

HCASMCs were seeded at 5×10^5 cells in a culture dish. After they reached confluence, cells were pretreated with vehicle or the indicated concentration (micromolar) of test drug for 10 min and then with vehicle or S1P (0.1 μM) for 3 min at 37°C. The amounts of activated Rho (GTP-Rho) were measured by a Rho Activation Assay Biochem Kit (Cytoskeleton, Denver, CO) according to the manufacturer's instructions. Quantitative analysis was performed as described above. The density ratio of GTP-Rho to total Rho was measured, and its vehicle value was set to 1.0.

Pharmacokinetic Analysis

Male SD rats were purchased from Nihon SLC. Blood samples were collected from the jugular vein at 1, 2, 4, 6, 8, and 24 h after the start of the administration of TY-52156-HCl. Samples were placed into sodium-heparinized tubes and subjected to centrifugation at 14,000*g* for 10 min at 4°C to separate the plasma. Plasma concentrations were quantified by an API 4000 LC/MS/MS System (Applied Biosystems/MDS Sciex, Foster City, CA). The mean peak plasma concentration (C_{max}) and time to reach C_{max} (T_{max}) were estimated from actual measurements. The half-life ($t_{1/2}$) was calculated with WinNonlin version 2.1 software (Pharsight, Mountain View, CA).

Measurement of Systemic Blood Pressure, Heart Rate, and Mean Blood Pressure

Male SD rats (290–340 g) were purchased from Nihon SLC. Systemic blood pressure (SBP) and heart rate (HR) were measured in the conscious state with a tail-cuff blood pressure analyzer (Muromachi-kikai, Tokyo, Japan). In another experiment, SD rats were anesthetized by the injection of pentobarbital (50 mg/kg i.p.), and cannulae were placed in a carotid artery and femoral vein. Mean blood pressure (MBP) was measured with a pressure transducer that was connected to the cannula placed in a carotid artery. HR was measured with a tachometer (NEC-San-ei Instruments, Tokyo, Japan). MBP and HR were measured before and 10 and 20 min after the injection of FTY-720 (1.0 mg/kg i.v.).

Statistical Analysis

Experimental values are expressed as mean ± S.E.M. The Student's *t* test or analysis of variance followed by Dunnett's multiple-comparison test was used to statistically analyze differences between groups. $P < 0.05$ was considered to be significant.

Results

TY-52156 Is a Potent $S1P_3$ Receptor Antagonist. $S1P_3$ receptor contributes to the S1P-induced increase in $[Ca^{2+}]_i$ (Ishii et al., 2002). To identify potent $S1P_3$ receptor antagonists, first, we screened a diverse compound collection (7500 compounds) by a Ca^{2+} fluorescent assay using $S1P_3$-CHO (see Supplementary Methods). The hit criterion was defined as more than 50% inhibition of the S1P (0.01 μM)-induced increase in $[Ca^{2+}]_i$ at 10 μM. Second, several possible compounds were pruned to confirm the dose-dependent and specific inhibition of $S1P_3$ receptor. Third, we synthesized derivatives of the active compounds to improve their potency and selectivity toward $S1P_3$ receptor. As a result, we identified TY-52156 as a potent $S1P_3$ receptor antagonist (Fig. 1A). TY-52156 preferentially inhibited the S1P-induced increase in $[Ca^{2+}]_i$ in $S1P_3$-CHO rather than $S1P_1$-, $S1P_2$-CHO, and $S1P_4$-Chem (Fig. 1B and Supplementary Fig. 1 as the direct ratio of fluorescence). The dose-dependent $[Ca^{2+}]_i$ increase elicited by S1P in $S1P_3$-CHO was inhibited by TY-52156 in a competitive manner (Fig. 1C), and the K_i value was estimated to be 110 nM for $S1P_3$ receptor.

In addition to S1P receptor-expressing cell lines, we used HUVECs to confirm the specificity of TY-52156 for endogenous $S1P_3$ receptor. $S1P_1$ and $S1P_3$ receptors but not other S1P receptors are expressed on HUVECs and induce $[Ca^{2+}]_i$ elevation (Sensken et al., 2008), which is consistent with the finding that TY-52156 and VPC23019 inhibited the S1P-induced increase in $[Ca^{2+}]_i$ in HUVECs (Supplementary Fig. S2). Furthermore, the combination of TY-52156 and VPC23019 showed greater inhibitory activity than either compound alone (Supplementary Fig. S2). Thus, S1P induces $[Ca^{2+}]_i$ elevation via $S1P_1$ and $S1P_3$ receptors in HUVECs. To assess the inhibitory effect of the TY-52156 on S1P-induced increase in $[Ca^{2+}]_i$ through $S1P_3$, but not $S1P_1$, receptor, the SEW2871 (an $S1P_1$ receptor-specific agonist)-induced increase in $[Ca^{2+}]_i$ in HUVECs was evaluated with or without TY-52156. Pre-

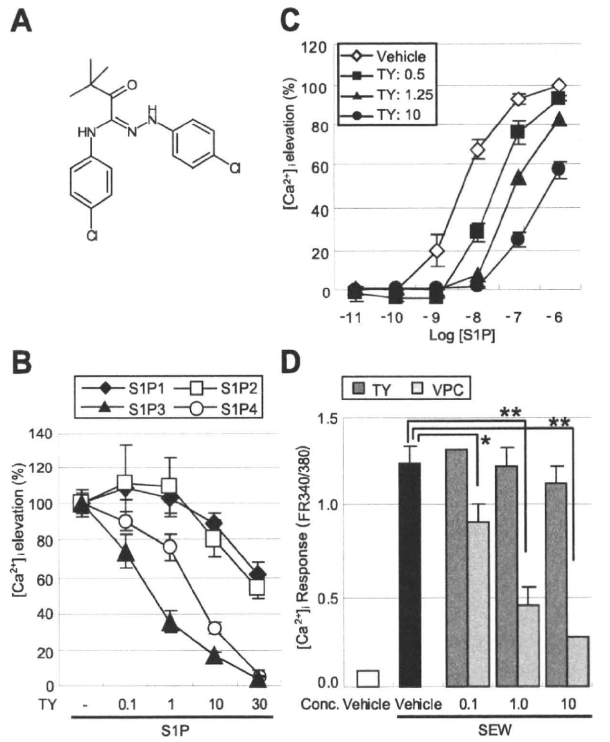

Fig. 1. Effects of S1P receptor antagonist on the S1P-induced increase in $[Ca^{2+}]_i$. A, chemical structure of TY-52156. B, $S1P_1$-, $S1P_2$-, $S1P_3$-CHO or $S1P_4$-Chem were pretreated with vehicle or the indicated concentration (micromolar) of test drug for 20 min and then treated with vehicle (−) or S1P (0.01 μM) to determine the increase in $[Ca^{2+}]_i$. The results are representative of three or four independent experiments. The relative percentage compared with the vehicle was calculated and expressed as mean ± S.E.M. C, $S1P_3$-CHO were pretreated with vehicle or the indicated concentration (micromolar) of TY-52156 for 20 min, and then treated with vehicle or the indicated concentration of S1P (logM) to determine the increase in $[Ca^{2+}]_i$. The relative percentage compared with the S1P (1 μM, vehicle treatment) was calculated and expressed as mean ± S.E.M. D, HUVECs were pretreated with vehicle or the indicated concentration (micromolar) of the test drug for 20 min, and then treated with vehicle or SEW2871 (SEW) (5.0 μM). The results are representative of three or four independent experiments. The ratio of the fluorescence intensity was calculated. The results are expressed as mean ± S.E.M. *, $P < 0.05$, **, $P < 0.01$ versus S1P alone (Dunnett's test).

treatment with VPC23019 (an $S1P_1$ receptor antagonist) significantly inhibited the SEW2871-induced increase in $[Ca^{2+}]_i$ through $S1P_1$ receptor (Fig. 1D). In contrast, this inhibition was blunted by pretreatment with TY-52156. These results suggest that TY-52156 inhibits the $S1P_3$ receptor-dependent increase in $[Ca^{2+}]_i$.

TY-52156 Is a Selective $S1P_3$ Receptor Antagonist. Using a [^{3}H]S1P binding assay, we found that TY-52156 inhibited the specific binding of [^{3}H]S1P to the membrane fraction of $S1P_3$-CHO in a dose-dependent manner (Fig. 2A). The total [^{3}H]S1P binding and nonspecific binding were 2156 ± 315 and 883 ± 109, respectively (mean dpm values ± S.E.M., $n = 5$). To further characterize the antagonist actions of TY-52156, we performed Eu-GTP binding to membranes prepared from cells expressing the human $S1P_1$, $S1P_2$, $S1P_3$, or $S1P_5$ receptors. The Eu-GTP binding assay has become a powerful alternative to the [^{35}S]GTPγS binding assay (Moreland et al., 2004). TY-52156 showed submicromolar potency and a high degree of selectivity for $S1P_3$ receptor (Fig. 2B).

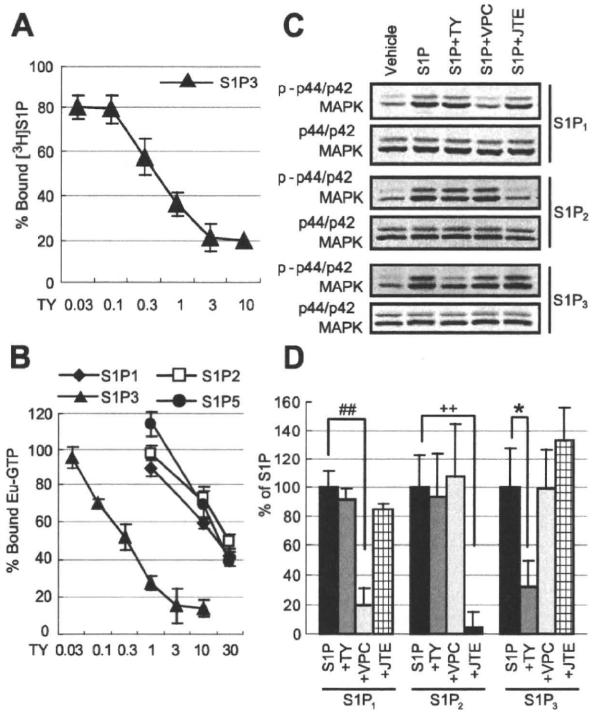

Fig. 2. Selectivity of TY-52156 toward $S1P_3$ receptor. A, the antagonistic effect of TY-52156 was determined by a radioligand binding study based on [^{3}H]S1P. Results are representative of three independent experiments. The relative percentage of specific binding compared with the vehicle was calculated and expressed as mean ± S.E.M. B, the antagonistic effect of TY-52156 was determined by a fluorescence-based Eu-GTP binding activity. The reaction was started by adding membranes containing human $S1P_1$, $S1P_2$, $S1P_3$, or $S1P_5$ receptors to the assay buffer including S1P (0.1 μM) and the desired concentration of TY-52156 (TY) (micromolar). The results are representative of three or four independent experiments. The relative percentage compared with the vehicle was calculated and expressed as mean ± S.E.M. C, $S1P_1$-, $S1P_2$-, or $S1P_3$-CHO were pretreated with vehicle, TY-52156 (TY) (10 μM), VPC23019 (VPC) (10 μM), or JTE013 (JTE) (1.0 μM) for 10 min and then treated with vehicle or S1P (0.1 μM) to determine p44/p42 MAPK phosphorylation. D, the data obtained from three independent experiments in C were quantitatively analyzed. ##, $P < 0.01$ versus S1P alone in $S1P_1$-CHO, ++, $P < 0.01$ versus S1P alone in $S1P_2$-CHO, *, $P < 0.05$ versus S1P alone in $S1P_3$-CHO (Dunnett's test).

We examined the selective inhibitory effect of TY-52156 on S1P-induced p44/p42 MAPK phosphorylation in $S1P_1$-, $S1P_2$- and $S1P_3$-CHO. TY-52156, VPC23019, and JTE013 inhibited S1P-induced p44/p42 MAPK phosphorylation only in $S1P_3$-, $S1P_1$-, and $S1P_2$-CHO, respectively (Fig. 2, C and D). Although VPC23019 is at least one-fifth less active toward $S1P_3$ receptor than $S1P_1$ receptor (Davis et al., 2005), it did not have an inhibitory effect on S1P-induced p44/p42 MAPK phosphorylation in $S1P_3$-CHO under our experimental conditions.

We further confirmed the selectivity of TY-52156 (10 μM) by examining its inhibitory effects on 24 GPCRs and three ion channels (all percentage inhibitions <30%, see Supplemental Table). These results indicate that TY-52156 is a potent $S1P_3$ receptor-selective antagonist.

S1P Reduces Coronary Flow via $S1P_3$ Receptor. S1P is released from activated platelets and thus is believed to be involved in thrombosis-related vascular diseases such as acute coronary syndrome (Siess, 2002). Recent studies have reported that intravenous injection of S1P decreases myocardial perfusion via $S1P_3$ receptor in vivo (Levkau et al., 2004). To investigate whether TY-52156 regulates CF, we examined its effect on S1P-dependent CF regulation. Consistent with previous reports (Sugiyama et al., 2000), we found that S1P dose-dependently decreased CF in perfused rat heart (Fig. 3A). Hearts were perfused with a solution containing each S1P receptor antagonist before S1P treatment. TY-52156, but not VPC23019 or JTE013, significantly restored the S1P-dependent reduction of CF (Fig. 3B). Meanwhile, TY-52156 did not affect the reduction of CF caused by a stable analog of thromboxane A_2, U46619. These results indicate that S1P reduces CF via $S1P_3$ receptor.

S1P Induces the Vasoconstriction of Canine Cerebral Arteries via $S1P_3$ Receptor. To investigate whether $S1P_3$ receptor expressed in the vasculature plays a role in S1P-induced vasoconstriction, we focused on the effect of TY-52156 on S1P-induced vasoconstriction in isolated canine cerebral arteries. S1P dose-dependently induced vasoconstriction (Fig. 4A), which is consistent with previous reports (Tosaka et al., 2001). TY-52156 cumulatively induced the relaxation of canine cerebral arteries that had been precontracted by S1P (Fig. 4B). These results suggest that S1P induces the vasoconstriction of isolated canine cerebral arteries via the $S1P_3$ receptor.

S1P Induces Both Rho Activation and the Increase in Ca^{2+} via $S1P_3$ Receptor in HCASMCs. Vascular tone balances relaxation and constriction in smooth muscle cells (Watterson et al., 2005). Vasorelaxation is mainly mediated by nitric oxide released from endothelial cells, where S1P activates endothelial nitric-oxide synthase. Vasoconstriction is presumably regulated by S1P-induced Rho activation and the increase in $[Ca^{2+}]_i$ in vascular smooth muscle cells. Because arteries were contracted by S1P stimulation, we assumed that S1P-mediated contraction dominated S1P-mediated relaxation in isolated perfused heart and arteries. Therefore, we hypothesized that the S1P-induced decrease in CF in isolated perfused rat heart might be ascribed to the contraction of coronary artery smooth muscle cells expressing $S1P_3$ receptor. We tested whether TY-52156 inhibited S1P-induced Rho activation and the increase in $[Ca^{2+}]_i$ in HCASMCs.

S1P-induced Rho activation in HCASMCs was inhibited by TY-52156 (Fig. 5A). JTE013 also inhibited S1P-induced Rho activation (Fig. 5B), which is consistent with previous studies (Arikawa et al., 2003). The combination of TY-52156 and JTE013 showed greater inhibitory activity than either compound alone (Fig. 5C). In contrast, VPC23019 did not inhibit S1P-induced Rho activation. SEW2871 did not induce Rho activation (Fig. 5D). Pretreatment with TY-52156 prevented the S1P-induced increase in $[Ca^{2+}]_i$ in HCASMCs (Fig. 6). Meanwhile, pretreatment with VPC23019, but not JTE013, attenuated the S1P-induced increase in $[Ca^{2+}]_i$ in HCASMCs. Collectively, these results suggest that $S1P_3$ receptor is responsible for both S1P-induced Rho activation and the increase in $[Ca^{2+}]_i$, whereas $S1P_1$ and $S1P_2$ receptors are involved in the increase in $[Ca^{2+}]_i$ and Rho activation, respectively.

TY-52156 Suppresses $S1P_3$ Receptor-Induced Bradycardia In Vivo. Finally, we sought to confirm the effects of TY-52156 in living animals. To test whether TY-52156 inhibits its $S1P_3$ receptor in vivo, we examined the antagonistic effects of TY-52156 on the FTY-720 (nonselective S1P receptor agonist)-induced transient reduction of HR.

The oral bioavailability of TY-52156 in SD rats was estimated to be 70.9% (Fig. 7A). To determine the pretreatment time before FTY-720 injection, the plasma concentrations of TY-52156 were measured (Fig. 7B). We also confirmed that oral administration of TY-52156 did not affect either HR or SBP in conscious rats (Fig. 7, C and D).

Although FTY-720 is a broad agonist of S1P receptors, it induces bradycardia, which has been shown to be mediated by the activation of $S1P_3$ receptor using $S1P_3$ receptor-null mice (Forrest et al., 2004; Sanna et al., 2004). FTY-720 (intravenous)-induced sinus bradycardia was observed from 10 to 20 min (Fig. 7E). Pretreatment with TY-52156 partially but significantly attenuated FTY-720-induced bradycardia but did not affect the FTY-720-induced elevation of MBP in unconscious rats (Fig. 7, E and F).

To complement the observation that TY-52156 inhibited FTY-720-induced bradycardia in vivo, dose-dependent inhibition of the FTY-720-induced cellular response was clarified. FTY-720 is phosphorylated to the active metabolite FTY-720 phosphate (FTY-720-P) in vivo (Zemann et al., 2006). We examined the inhibitory effect of TY-52156 on the FTY-720-P-induced increase in $[Ca^{2+}]_i$ in $S1P_3$-CHO. Pretreatment with TY-52156 prevented the FTY-720-P-induced increase in $[Ca^{2+}]_i$ in a dose-dependent manner (Fig. 8). Collectively, these results indicate that the oral administration of TY-52156 inhibits $S1P_3$ receptor-dependent bradycardia in vivo.

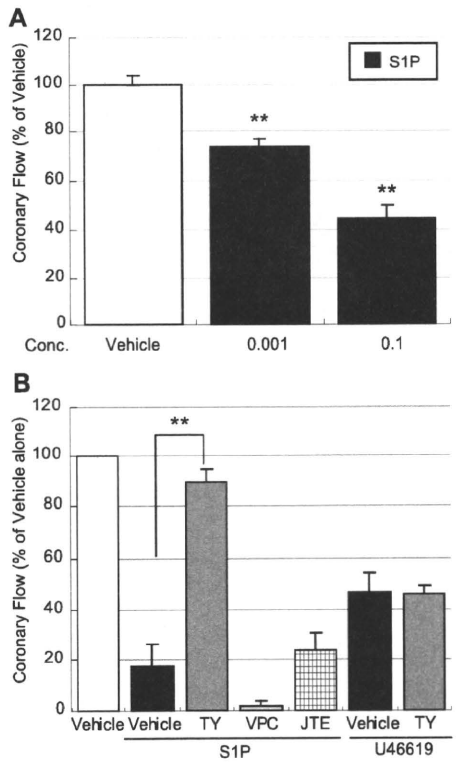

Fig. 3. Effects on the S1P- or U46619-induced change in cardiac coronary flow in isolated perfused rat hearts. A and B, isolated rat hearts were perfused at 37°C in a Langendorff manner with Krebs-Henseleit bicarbonate buffer at a constant perfusion pressure (70 ± 5 mm Hg). A, S1P dose-dependently (0.001 or 0.1 μM) decreased CF. Results are representative of five independent experiments. **, $P < 0.01$ versus vehicle (Dunnett's test). B, perfused rat hearts were pretreated with TY-52156 (TY) (0.1 μM), VPC23019 (VPC) (0.1 μM), or JTE013 (JTE) (0.1 μM) for 10 min and then treated with vehicle, S1P (0.1 μM), or U46619 (0.1 μM). Results are representative of five independent experiments. **, $P < 0.01$ versus S1P alone (Dunnett's test).

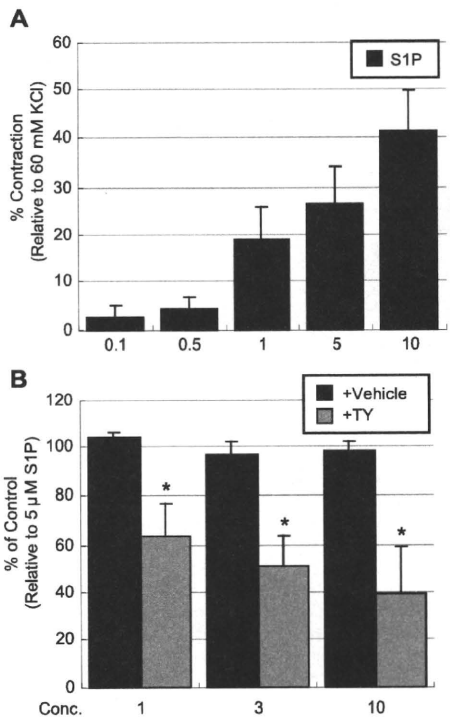

Fig. 4. Effects of TY-52156 on the S1P-induced contractile response in isolated canine cerebral arteries. A, S1P dose-dependently (0.1 to 10 μM) induced vasoconstriction in isolated canine cerebral arteries. Results are representative of three independent experiments. B, canine cerebral arteries were contracted by S1P (5.0 μM). After the maximum contractile response was observed, an increasing amount of TY-52156 (up to 10 μM) was applied to the organ chambers. Relaxation responses were measured every 10 min after the addition of the indicated concentration of vehicle or TY-52156 (micromolar). Results are representative of four independent experiments. *, $P < 0.05$, versus indicated dose of vehicle (Student's t test).

Discussion

TY-52156 was identified as a potent and selective antagonist of $S1P_3$ receptor. Based on its ability to inhibit Ca^{2+} responses and the results of an Eu-GTP binding assay, TY-52156 was approximately 10 to 30 times more potent for $S1P_3$ receptor than for $S1P_1$, $S1P_2$, $S1P_4$, or $S1P_5$ receptor, and the K_i value for $S1P_3$ receptor was estimated to be 110 nM. TY-52156 caused a parallel rightward shift of the dose-response curve for the S1P-induced increase in $[Ca^{2+}]_i$, which suggested competitive antagonism for $S1P_3$ receptor. Furthermore, TY-52156 did not have any significant effects on 24 GPCRs or three ion channels. Therefore, TY-52156 is a useful tool for studying $S1P_3$ receptor signaling.

VPC23019 has been described as an $S1P_1$ and $S1P_3$ receptor antagonist, with pK_b values (−logM) of 7.49 ± 0.15 and 5.98 ± 0.08 for the $S1P_1$ and $S1P_3$ receptors, respectively (Davis et al., 2005). Although VPC23019 (10 μM) did not inhibit p44/p42 MAPK phosphorylation in $S1P_3$-CHO, dose-dependent inhibition was observed at higher concentrations (30–100 μM) (Supplementary Fig. 3A). On the other hand, VPC23019 dose-dependently inhibited Eu-GTP binding to membranes ($S1P_3$) from 1 to 10 μM (Supplementary Fig. 3B), which is similar to previous findings (Davis et al., 2005). One possible explanation is that VPC23019 did not inhibit the cellular response on $S1P_3$-CHO because of the difference in sensitivity between membrane-based and whole cell-based assay conditions. In addition, because VPC23019 has been characterized in T24 cells (human bladder carcinoma) that stably expressed $S1P_3$ receptor (Davis et al., 2005), host-cell–specific differences between T24 cells and our Chinese hamster ovary K1 cells might play a role.

We demonstrated that $S1P_3$ receptor is central to S1P-regulated CF. CF is increased or decreased physiologically in response to the oxygen demand of the heart muscle. Thrombosis and atherosclerosis decrease CF by releasing S1P, thromboxane A_2, and platelet-derived growth factor from activated platelets and by narrowing the lumen of the coronary arteries, respectively (Pomposiello et al., 1997; Heldin and Westermark, 1999). Although S1P has been reported to decrease CF, it is not well known how S1P induces vasoconstriction. The deletion of $S1P_3$ receptor in mice led to inhibition of the S1P-induced decrease in myocardial perfusion (Levkau et al., 2004). We found that TY-52156, but not VPC23019 or JTE013, attenuated the S1P-dependent reduction of CF. Therefore, $S1P_3$ receptor is responsible for the S1P-induced decrease in cardiac coronary flow. Because $S1P_3$ receptor is highly expressed in the smooth muscle of small coronary vessels (Himmel et al., 2000; Mazurais et al., 2002), reduction of CF by S1P may primarily depend on the vasoconstriction of microvascular smooth muscle cells.

We focused on the mechanism by which $S1P_3$ receptor regulates the contraction of smooth muscle cells. There are two main signals that induce actomyosin-based contraction: an increase in $[Ca^{2+}]_i$, and Rho activation (Watterson et al., 2005). We observed that TY-52156 inhibited the S1P-induced increase in $[Ca^{2+}]_i$ and Rho activation in HCASMCs. In clear contrast, VPC23019 and JTE013 only inhibited the increase in $[Ca^{2+}]_i$ and Rho activation, respectively. Thus, $S1P_3$ receptor-mediated signal through both the increase in $[Ca^{2+}]_i$ and Rho activation, which lead to vasoconstriction, can account for our finding that TY-52156, but not VPC23019 or JTE013, preserved the S1P-dependent reduction of CF in perfused rat heart. Although Rho kinase inhibition has been believed to cause vasorelaxation (Tosaka et al., 2001), it is unclear why JTE013 did not alter the S1P-dependent reduction of CF. One possible explanation is the difference in the expression of S1P receptor subtypes in the vasculature (Coussin et al., 2002; Mazurais et al., 2002).

Sustained vascular spasm after subarachnoid hemorrhage and cerebral infarction has been shown to result in the extension of brain damage (Tosaka et al., 2001). The involvement of $S1P_3$ receptor in vasospasm has been reported using $S1P_3$ receptor-null mice (Salomone et al., 2008). The intracarotid injection of S1P decreases cerebral blood flow in vivo (Salomone et al., 2003). Thus, TY-52156 may potentially inhibit the S1P-induced vasospasm of cerebral arteries, because we found that TY-52156 attenuated S1P-induced vascular contraction in canine cerebral arteries.

S1P has opposite effects on vasculature: vasorelaxation and vasoconstriction. $S1P_1$ and $S1P_3$ receptors have been linked to the activation of NO synthesis in vascular endothelial cells (Igarashi and Michel, 2000; Dantas et al., 2003; Nofer et al., 2004). However, we confirmed that activation of $S1P_3$ receptor led to vasoconstriction in smooth muscle cells. Therefore, the net effect of $S1P_3$ receptor on vasorelaxation and vasoconstriction depends on the function of vascular endothelial cells or the expression profile of S1P receptor subtypes in the vasculature (Fig. 9). Endothelial-dependent vasorelaxation is supported by the fact that various vasoconstrictors, including acetylcholine and ergonovine, cause endothelium-dependent vasorelaxation via a NO-dependent mechanism in healthy subjects (Kugiyama et al., 1996; Davignon and Ganz, 2004; Kawano and Ogawa, 2004). This vasorelaxation is impaired in patients with endothelial dysfunction. Thus, S1P at least contributes to pathological processes that involve endothelial dysfunction, such as vasospasm and myocardial infarction.

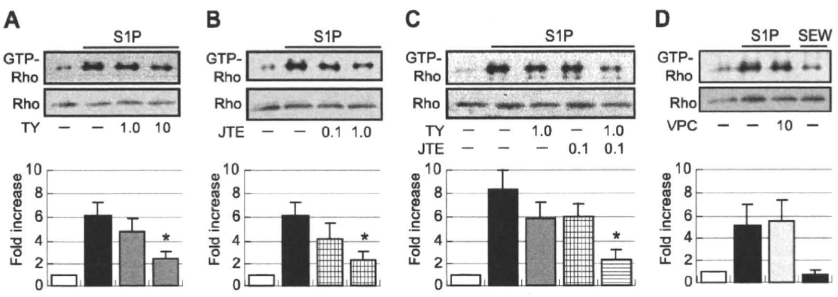

Fig. 5. Effects of S1P receptor antagonist on S1P-induced Rho activation in HCASMCs. HCASMCs were pretreated with vehicle or the indicated concentration (micromolar) of test the drug for 10 min, and further treated with vehicle, S1P (1.0 μM) or SEW2871 (SEW) (10 μM) for 3 min. The data obtained from three (A, B, and D) or four (C) independent experiments were quantitatively analyzed (bottom). *, $P < 0.05$, versus S1P alone (Dunnett's test).

TY-52156 might become a potent probe for assessing $S1P_3$ receptor-dependent signal in vivo. FTY-720 binds to all S1P receptors except for $S1P_2$ receptor (Huwiler and Pfeilschifter, 2008). Although FTY-720-induced bradycardia is mainly caused by the $S1P_3$ receptor-mediated activation of cardiac G protein-gated potassium channel (Ik_{Ach}), it has been reported to be associated with Ik_{Ach}-independent mechanisms through FTY-720 induction (Himmel et al., 2000; Forrest et al., 2004; Koyrakh et al., 2005). Based on the study of Ik_{Ach}-deficient mice, other pacing-related currents such as the hyperpolarization-activated inward current and the voltage-gated calcium current may be involved in the bradycardia with FTY-720 (Koyrakh et al., 2005). In addition, despite the lack of $S1P_3$ receptor agonism, a recent clinical study has reported that a selective $S1P_1/S1P_5$ receptor agonist (BAF-312, the structure of which has not been disclosed) decreased the heart rate in healthy subjects (Gergely et al., 2009). Our result showed that FTY-720 (intravenous) decreased HR and elevated MBP in rats. Pretreatment with TY-52156 before FTY-720 partially restored the FTY-720-induced HR reduction but did not attenuate the elevation of MBP. Because the oral administration of TY-52156 alone did not affect HR or SBP in conscious rats, this result probably means that there is no effect on hyperpolarization-activated inward current to modulate HR. We also found that TY-52156 did not affect voltage-gated calcium current in guinea pig ventricular myocytes (Supplemental Table). Thus, these results indicated that FTY-720-induced bradycardia may be involved in the mechanism, except through $S1P_3$ receptor. Although FTY-720 induced an elevation of MBP in a clinical study, the mechanism was not clear (Kappos et al., 2006). Therefore, TY-52156 inhibits $S1P_3$ receptor-dependent HR reduction in vivo and thus is

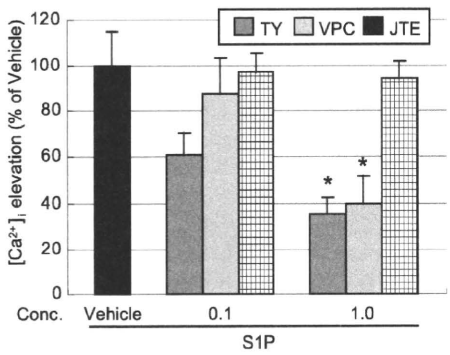

Fig. 6. Effects of S1P receptor antagonist on the S1P-induced increase in $[Ca^{2+}]_i$ in HCASMCs. HCASMCs were pretreated with vehicle or the indicated concentration (micromolar) of the test drug for 20 min, and further treated with vehicle or S1P (0.01 μM). Results are representative of three or four independent experiments. The relative percentage compared with the vehicle was calculated and expressed as mean ± S.E.M. *, $P < 0.05$, versus S1P alone (Dunnett's test).

A

	Administration Route	
	Oral	Intravenous
Dose (mg/kg)	1.0	0.02
AUC (ng·mL/min)	26,659 ± 5,847	710 ± 343
Bioavailability (%)	70.9	

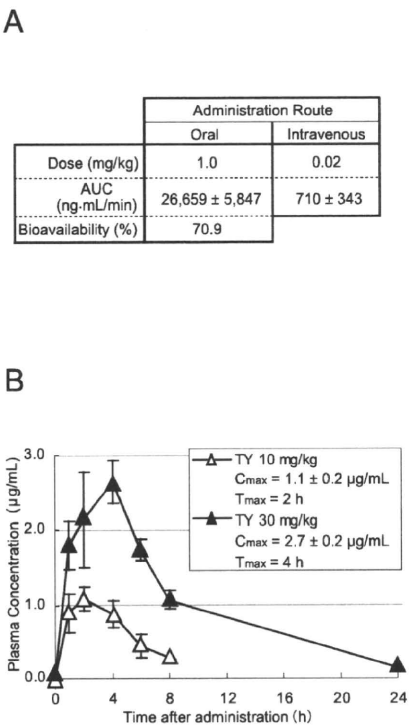

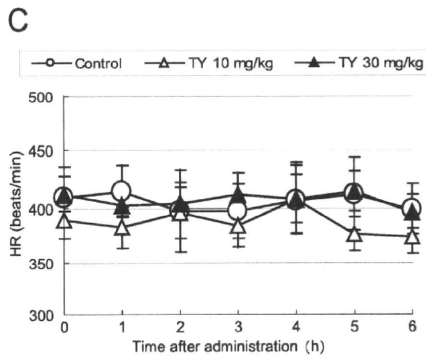

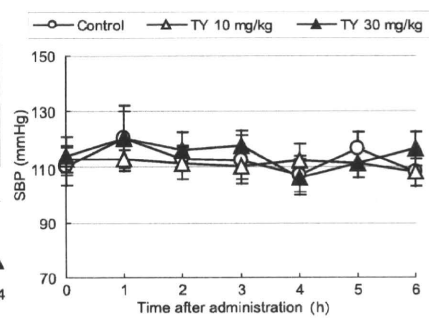

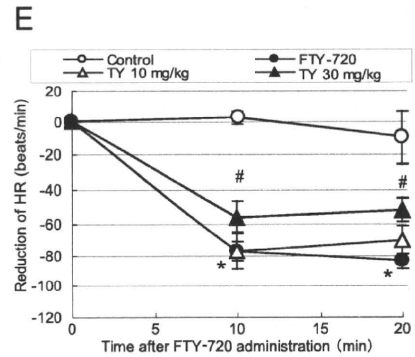

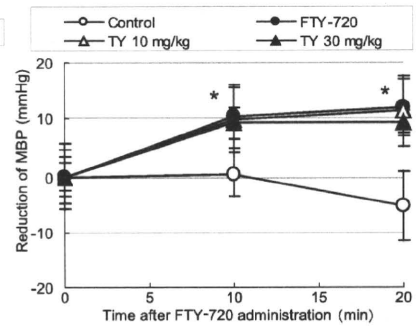

Fig. 7. Effects of TY-52156 on FTY-720-induced bradycardia and hypertension in SD rat. A, the oral bioavailability of TY-52156 was studied in SD rats. The plasma concentration of TY-52156 was determined by LC/MS/MS. Area under the blood concentration curve (AUC) from 0 to 360 min was calculated using a trapezoidal rule. The results are expressed as mean ± S.D. B, the plasma concentration of TY-52156 after oral administration was determined by LC/MS/MS. The dose of TY-52156 (TY) was 10 (△) or 30 mg/kg (▲). The results are expressed as mean ± S.D. for three SD rats. C and D, changes in HR (C) and SBP (D) were recorded after the oral administration of TY-52156 (TY) (10 mg/kg, △; or 30 mg/kg, ▲) or control (○) in conscious rats. Results are representative of five independent experiments. E and F, changes in HR (E) and MBP (F) were recorded after the administration of FTY-720 (1.0 mg/kg i.v.; ●) or control (○) in anesthetized rats. TY-52156 (TY) (10 mg/kg, △; or 30 mg/kg, ▲) was administered orally at 4 h before FTY-720 injection. Results are representative of six independent experiments. *, $P < 0.05$ versus control (unpaired Student's t test). #, $P < 0.05$ versus FTY-720 alone (Dunnett's test).

a potent probe for elucidating the role of $S1P_3$ receptor in animal models.

In conclusion, TY-52156 is a potent and selective antagonist of $S1P_3$ receptor. This compound may help us to distinguish $S1P_3$ receptor-dependent signals from $S1P_1$ and $S1P_2$ receptor-dependent signals in vitro and in vivo. $S1P_3$ receptor is responsible for the S1P-induced decrease in CF, and an $S1P_3$ receptor antagonist may be useful for the treatment of S1P-induced vascular diseases, including vasospasm.

Acknowledgments

We thank Yumi Kato and Akemi Furukawa-Yoshida (Fukushima Research Laboratories, TOA EIYO Ltd., Saitama, Japan) for technical assistance.

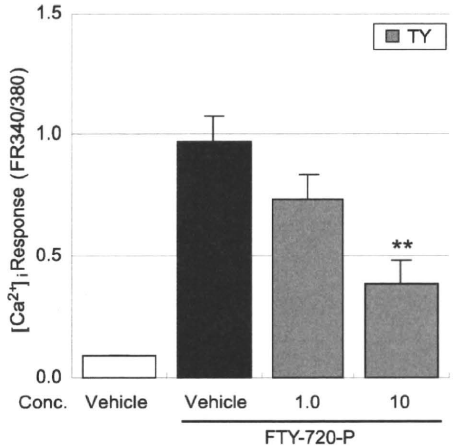

Fig. 8. Effects of TY-52156 on the FTY-720-P-induced increase in $[Ca^{2+}]_i$ in $S1P_3$-CHO. $S1P_3$-CHO were pretreated with vehicle or the indicated concentration (micromolar) of TY-52156 (TY) for 20 min and further treated with vehicle or FTY-720-P (0.5 μM). The results are representative of five independent experiments. The ratio of the fluorescence intensity was calculated. The relative percentage compared with the vehicle was calculated and expressed as mean ± S.E.M. *, $P < 0.05$, versus FTY-720-P alone (Dunnett's test).

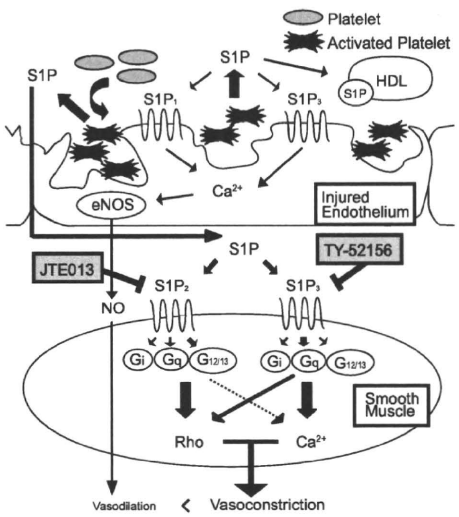

Fig. 9. Summary of signaling pathways for S1P-induced vasoconstriction. S1P causes vasoconstriction in smooth muscle cells via $S1P_2$ and $S1P_3$ receptors. Inhibition of both the increase in $[Ca^{2+}]_i$ and Rho activation contributes to the efficacy of TY-52156 against S1P-induced vasoconstriction.

References

Arikawa K, Takuwa N, Yamaguchi H, Sugimoto N, Kitayama J, Nagawa H, Takehara K, and Takuwa Y (2003) Ligand-dependent inhibition of B16 melanoma cell migration and invasion via endogenous S1P2 G protein-coupled receptor. Requirement of inhibition of cellular RAC activity. *J Biol Chem* **278:**32841–32851.

Coussin F, Scott RH, Wise A, and Nixon GF (2002) Comparison of sphingosine 1-phosphate-induced intracellular signaling pathways in vascular smooth muscles: differential role in vasoconstriction. *Circ Res* **91:**151–157.

Dantas AP, Igarashi J, and Michel T (2003) Sphingosine 1-phosphate and control of vascular tone. *Am J Physiol Heart Circ Physiol* **284:**H2045–2052.

Davignon J and Ganz P (2004) Role of endothelial dysfunction in atherosclerosis. *Circulation* **109:**III27–III32.

Davis MD, Clemens JJ, Macdonald TL, and Lynch KR (2005) Sphingosine 1-phosphate analogs as receptor antagonists. *J Biol Chem* **280:**9833–9841.

Forrest M, Sun SY, Hajdu R, Bergstrom J, Card D, Doherty G, Hale J, Keohane C, Meyers C, Milligan J, et al. (2004) Immune cell regulation and cardiovascular effects of sphingosine 1-phosphate receptor agonists in rodents are mediated via distinct receptor subtypes. *J Pharmacol Exp Ther* **309:**758–768.

Gergely P, Wallström E, Nuesslein-Hildesheim B, Bruns C, Zécri F, Cooke N, Traebert M, Tuntland T, Rosenberg M and Saltzman M (2009) Phase I study with the selective S1P1/S1P5 receptor modulator BAF312 indicates that S1P1 rather than S1P3 mediates transient heart rate reduction in humans. *Multiple Sclerosis* **15 (9 Suppl):**S235–S236.

Heldin CH and Westermark B (1999) Mechanism of action and in vivo role of platelet-derived growth factor. *Physiol Rev* **79:**1283–1316.

Himmel HM, Meyer Zu Heringdorf D, Graf E, Dobrev D, Kortner A, Schüler S, Jakobs KH, and Ravens U (2000) Evidence for Edg-3 receptor-mediated activation of I(K.ACh) by sphingosine-1-phosphate in human atrial cardiomyocytes. *Mol Pharmacol* **58:**449–454.

Huwiler A and Pfeilschifter J (2008) New players on the center stage: sphingosine 1-phosphate and its receptors as drug targets. *Biochem Pharmacol* **75:**1893–1900.

Igarashi J and Michel T (2000) Agonist-modulated targeting of the EDG-1 receptor to plasmalemmal caveolae. eNOS activation by sphingosine 1-phosphate and the role of caveolin-1 in sphingolipid signal transduction. *J Biol Chem* **275:**32363–32370.

Ishii I, Ye X, Friedman B, Kawamura S, Contos JJ, Kingsbury MA, Yang AH, Zhang G, Brown JH, and Chun J (2002) Marked perinatal lethality and cellular signaling deficits in mice null for the two sphingosine 1-phosphate (S1P) receptors, S1P(2)/LP(B2)/EDG-5 and S1P(3)/LP(B3)/EDG-3. *J Biol Chem* **277:**25152–25159.

Kappos L, Antel J, Comi G, Montalban X, O'Connor P, Polman CH, Haas T, Korn AA, Karlsson G, Radue EW, et al. (2006) Oral fingolimod (FTY720) for relapsing multiple sclerosis. *N Engl J Med* **355:**1124–1140.

Kawano H and Ogawa H (2004) Endothelial dysfunction and coronary artery spasm. *Curr Drug Targets Cardiovasc Haematol Disord* **4:**23–33.

Koide Y, Uemoto K, Hasegawa T, Sada T, Murakami A, Takasugi H, Sakurai A, Mochizuki N, Takahashi A, and Nishida A (2007) Pharmacophore-based design of sphingosine 1-phosphate-3 receptor antagonists that include a 3,4-dialkoxybenzophenone scaffold. *J Med Chem* **50:**442–454.

Koyrakh L, Roman MI, Brinkmann V, and Wickman K (2005) The heart rate decrease caused by acute FTY720 administration is mediated by the G protein-gated potassium channel I. *Am J Transplant* **5:**529–536.

Kugiyama K, Yasue H, Okumura K, Ogawa H, Fujimoto K, Nakao K, Yoshimura M, Motoyama T, Inobe Y, and Kawano H (1996) Nitric oxide activity is deficient in spasm arteries of patients with coronary spastic angina. *Circulation* **94:**266–271.

Levkau B, Hermann S, Theilmeier G, van der Giet M, Chun J, Schober O, and Schäfers M (2004) High-density lipoprotein stimulates myocardial perfusion in vivo. *Circulation* **110:**3355–3359.

Lim HS, Oh YS, Suh PG, and Chung SK (2003) Syntheses of sphingosine-1-phosphate stereoisomers and analogues and their interaction with EDG receptors. *Bioorg Med Chem Lett* **13:**237–240.

Mazurais D, Robert P, Gout B, Berrebi-Bertrand I, Laville MP, and Calmels T (2002) Cell type-specific localization of human cardiac S1P receptors. *J Histochem Cytochem* **50:**661–670.

Moreland RB, Terranova MA, Chang R, Uchic ME, Matulenko MA, Surber BW, Stewart AO, and Brioni JD (2004) [^{3}H] A-369508 ([2-[4-(2-cyanophenyl)-1-piperazinyl]-*N*-(3-methylphenyl) acetamide]: an agonist radioligand selective for the dopamine D4 receptor. *Eur J Pharmacol* **497:**147–154.

Nofer JR, van der Giet M, Tölle M, Wolinska I, von Wnuck Lipinski K, Baba HA, Tietge UJ, Gödecke A, Ishii I, Kleuser B, et al. (2004) HDL induces NO-dependent vasorelaxation via the lysophospholipid receptor S1P3. *J Clin Invest* **113:**569–581.

Ohmori T, Yatomi Y, Osada M, Kazama F, Takafuta T, Ikeda H, and Ozaki Y (2003) Sphingosine 1-phosphate induces contraction of coronary artery smooth muscle cells via S1P2. *Cardiovasc Res* **58:**170–177.

Ohta H, Sato K, Murata N, Damirin A, Malchinkhuu E, Kon J, Kimura T, Tobo M, Yamazaki Y, Watanabe T, et al. (2003) Ki16425, a subtype-selective antagonist for EDG-family lysophosphatidic acid receptors. *Mol Pharmacol* **64:**994–1005.

Pomposiello S, Yang XP, Liu YH, Surakanti M, Rhaleb NE, Sevilla M, and Carretero OA (1997) Autacoids mediate coronary vasoconstriction induced by nitric oxide synthesis inhibition. *J Cardiovasc Pharmacol* **30:**599–606.

Rosen H, Gonzalez-Cabrera PJ, Sanna MG, and Brown S (2009) Sphingosine 1-phosphate receptor signaling. *Annu Rev Biochem* **78:**743–768.

Ryu Y, Takuwa N, Sugimoto N, Sakurada S, Usui S, Okamoto H, Matsui O, and Takuwa Y (2002) Sphingosine-1-phosphate, a platelet-derived lysophospholipid mediator, negatively regulates cellular Rac activity and cell migration in vascular smooth muscle cells. *Circ Res* **90:**325–332.

Salomone S, Potts EM, Tyndall S, Ip PC, Chun J, Brinkmann V, and Waeber C (2008) Analysis of sphingosine 1-phosphate receptors involved in constriction of isolated cerebral arteries with receptor null mice and pharmacological tools. *Br J Pharmacol* **153:**140–147.

Salomone S, Yoshimura S, Reuter U, Foley M, Thomas SS, Moskowitz MA, and

Waeber C (2003) S1P3 receptors mediate the potent constriction of cerebral arteries by sphingosine-1-phosphate. *Eur J Pharmacol* **469:**125–134.
Sanna MG, Liao J, Jo E, Alfonso C, Ahn MY, Peterson MS, Webb B, Lefebvre S, Chun J, Gray N, et al. (2004) Sphingosine 1-phosphate (S1P) receptor subtypes S1P1 and S1P3, respectively, regulate lymphocyte recirculation and heart rate. *J Biol Chem* **279:**13839–13848.
Sensken SC, Stäubert C, Keul P, Levkau B, Schöneberg T, and Gräler MH (2008) Selective activation of G alpha i mediated signalling of S1P3 by FTY720-phosphate. *Cell Signal* **20:**1125–1133.
Siess W (2002) Athero- and thrombogenic actions of lysophosphatidic acid and sphingosine-1-phosphate. *Biochim Biophys Acta* **1582:**204–215.
Sugimoto N, Takuwa N, Okamoto H, Sakurada S, and Takuwa Y (2003) Inhibitory and stimulatory regulation of Rac and cell motility by the G12/13-Rho and Gi pathways integrated downstream of a single G protein-coupled sphingosine-1-phosphate receptor isoform. *Mol Cell Biol* **23:**1534–1545.
Sugiyama A, Yatomi Y, Ozaki Y, and Hashimoto K (2000) Sphingosine 1-phosphate induces sinus tachycardia and coronary vasoconstriction in the canine heart. *Cardiovasc Res* **46:**119–125.
Takuwa Y, Okamoto Y, Yoshioka K, and Takuwa N (2008) Sphingosine-1-phosphate signaling and biological activities in the cardiovascular system. *Biochim Biophys Acta* **1781:**483–488.
Tosaka M, Okajima F, Hashiba Y, Saito N, Nagano T, Watanabe T, Kimura T, and Sasaki T (2001) Sphingosine 1-phosphate contracts canine basilar arteries in vitro and in vivo: possible role in pathogenesis of cerebral vasospasm. *Stroke* **32:**2913–2919.
Watterson KR, Ratz PH, and Spiegel S (2005) The role of sphingosine-1-phosphate in smooth muscle contraction. *Cell Signal* **17:**289–298.
Yatomi Y (2006) Sphingosine 1-phosphate in vascular biology: possible therapeutic strategies to control vascular diseases. *Curr Pharm Des* **12:**575–587.
Zemann B, Kinzel B, Müller M, Reuschel R, Mechtcheriakova D, Urtz N, Bornancin F, Baumruker T, and Billich A (2006) Sphingosine kinase type 2 is essential for lymphopenia induced by the immunomodulatory drug FTY720. *Blood* **107:**1454–1458.

Address correspondence to: Dr. Akira Murakami, Drug Research Department, Tokyo Research Laboratories, TOA EIYO Ltd., 2-293-3 Amanuma, Omiya, Saitama 330-0834, Japan. E-mail: murakami.akira@toaeiyo.co.jp

Biochemical and Biophysical Research Communications 392 (2010) 150–154

Contents lists available at ScienceDirect

Biochemical and Biophysical Research Communications

journal homepage: www.elsevier.com/locate/ybbrc

PSF3 marks malignant colon cancer and has a role in cancer cell proliferation

Yumi Nagahama [a], Masaya Ueno [a,b], Naotsugu Haraguchi [c], Masaki Mori [c], Nobuyuki Takakura [a,*]

[a] Department of Signal Transduction, Research Institute for Microbial Diseases, Osaka University, 3-1 Yamadaoka, Suita, Osaka 565-0871, Japan
[b] Department of Molecular, Cell and Developmental Biology, University of California, Los Angeles, CA 90095, USA
[c] Department of Gastroenterological Surgery, Graduate School of Medicine, Osaka University, 2-2 Yamadaoka, Suita, 565-0871, Japan

ARTICLE INFO

Article history:
Received 22 December 2009
Available online 6 January 2010

Keywords:
PSF3
Colon carcinoma

ABSTRACT

PSF3 (partner of Sld five 3) is a member of the tetrameric complex termed GINS, composed of SLD5, PSF1, PSF2, and PSF3, and well-conserved evolutionarily. Previous studies suggested that some GINS complex members are upregulated in cancer, but PSF3 expression in colon carcinoma has not been investigated. Here, we established a mouse anti-PSF3 antibody, and examined PSF3 expression in human colon carcinoma cell lines and colon carcinoma specimens. We found that PSF3 is expressed in the crypt region in normal colonic mucosa and that many PSF3-positive cells co-expressed Ki-67. This suggests that PSF3-positivity of normal mucosa is associated with cell proliferation. Expression of the PSF3 protein was greater in carcinoma compared with the adjacent normal mucosa, and even stronger in high-grade malignancies, suggesting that it may be associated with colon cancer progression. PSF3 gene knock-down in human colon carcinoma cell lines resulted in growth inhibition characterized by delayed S-phase progression. These results suggest that PSF3 is a potential biomarker for diagnosis of progression in colon cancer and could be a new target for cancer therapy.

Introduction

PSF3 (partner of Sld five 3) is a member of the highly evolutionarily conserved tetrameric complex termed GINS, composed of SLD5, PSF1, PSF2, and PSF3. In yeast, the GINS complex associates with the Minichromosome maintenance (MCM) 2–7 complex and with CDC45, and this "C–M–G complex" (CDC45–MCM-2–7–GINS) regulates both the initiation and progression of DNA replication [1–6]. Thus, it has been suggested that GINS is involved in DNA replication in *Xenopus* and human [7–10]. However, a recent study suggested that PSF1/2 is associated with the response to replication stress and acquisition of DNA damage in untransformed human dermal fibroblasts [11]. As it has been reported that DNA replication-associated protein in yeast has diverse functions in different cells, e.g. origin recognition protein Orc1 has a role in determining centrosome copy number [12], the exact functions of GINS components in mammalian cells are not yet clear.

We have previously cloned the mouse ortholog of *PSF1* (partner of SLD5) from a hematopoietic stem cell (HSC) cDNA library [13] and found that *PSF1* expression in mice was predominantly observed in the adult BM and thymus, as well as the testis and ovary, i.e. tissues in which stem cell proliferation is actively induced and continues after birth. Moreover, we reported that PSF1 is strongly expressed in several immature cell lineages such as cells in the inner cell mass during early embryogenesis, and spermatogonia as well as HSCs after birth [13–15]. Loss of *PSF1* led to embryonic lethality around the implantation stage caused by the inability of cells of the inner cell mass to proliferate [13]. Moreover, haploinsufficiency of PSF1 in $PSF1^{+/-}$ mice resulted in the delayed induction of HSC proliferation during reconstitution of bone marrow after 5-FU ablation. These data strongly suggested that PSF1 is required for acute proliferation of cells, especially immature cells such as stem cells and progenitor cells. However, the role of the other components of GINS in mammalian cells has not been well determined.

Several recent reports have suggested a role for GINS components in cancer cells. For example, all GINS components were found to be overexpressed in intrahepatic cholangiocarcinoma tissues [16]. In a Gene Expression Omnibus (GEO) database search, *PSF1* was identified as an estrogen target in MCF7 human breast carcinoma cells [17]. In a comprehensive study, it was found that *PSF1* and *SLD5* were upregulated in aggressive melanoma [18].

Although several studies have suggested that GINS components play a role in cancer as described above, their expression in colon carcinoma has not been examined. Among the GINS complex members, the expression and role of PSF3 has not been well-documented because no appropriate antibody was available thus far. Therefore, we generated such an antibody against PSF3 and

Abbreviations: GINS, Go-ichi-nii-san; PSF, Partner of Sld five.

* Corresponding author. Fax: +81 6 6879 8314.
E-mail address: ntakaku@biken.osaka-u.ac.jp (N. Takakura).

0006-291X/$ - see front matter © 2010 Elsevier Inc. All rights reserved.
doi:10.1016/j.bbrc.2009.12.174

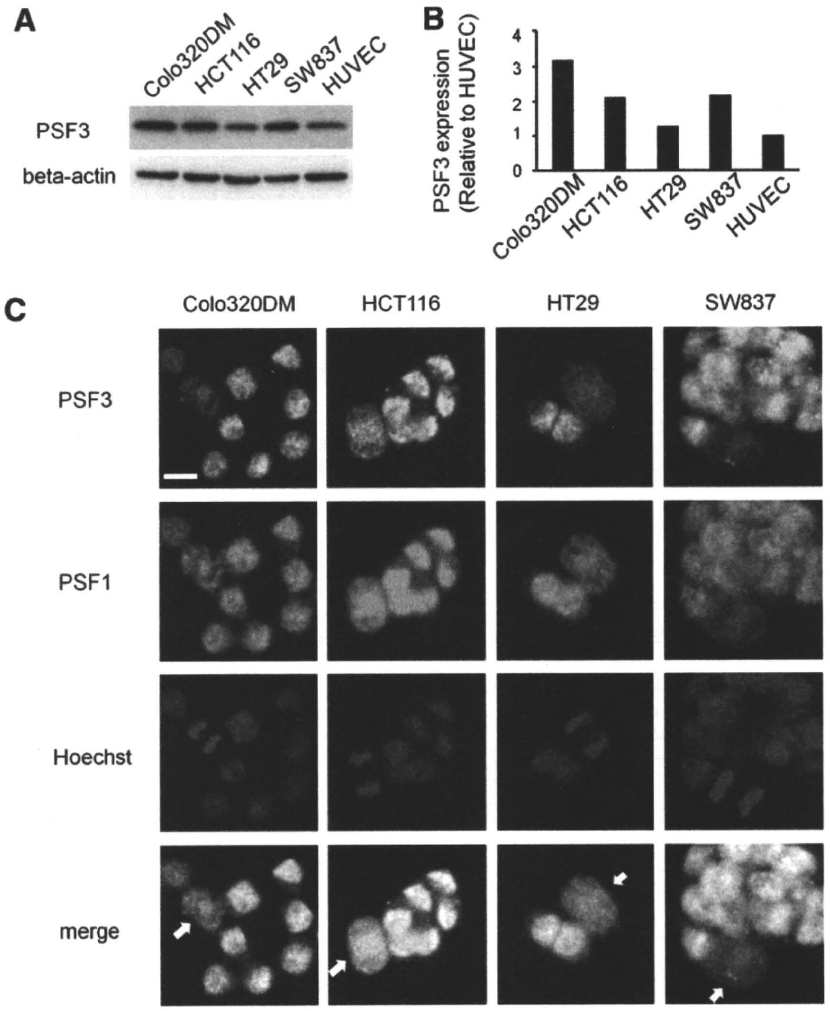

Fig. 1. PSF3 expression in human colon carcinoma cell lines. (A,B) Western blotting of PSF3 expression in whole cell extracts of each cell line as indicated. A representative result of Western blotting (A) and densitometric analysis for quantitative evaluation (B) are shown. (C) Cells as indicated were stained with anti-PSF3 antibody labeled with Alexa488 (green) and co-stained with anti-PSF1 antibody labeled with Cy3 (red). DNA was counter-stained with Hoechst (blue). Arrows, mitotic cells. Bar, 10 μm.

examined its reactivity with human colon carcinoma specimens. Furthermore, we silenced the *PSF3* gene by RNAi methodology to determine the impact of PSF3 knock-down on the growth of human colon carcinoma cell lines.

Materials and methods

Generation of anti-PSF3 antibody. For the generation of monoclonal anti-PSF3 antibody, PSF3 cDNA, coding full-length amino acid residues, was amplified by polymerase chain reaction (PCR), and then DNA fragments were ligated into pGEX-2T vector (Pharmacia Piscataway, NJ) for the preparation of glutathione *S*-transferase (GST)-fusion proteins. Purified GST-fused protein was used as antigen for mouse immunization, and hybridoma cells were established by standard procedures. Finally, stable hybridoma cell lines were obtained and cloned as aps3.2 and aps3.14. In this current study, aps3.2 was used. The specificities of the antibodies were analyzed by Western blotting and immunocytochemistry.

Cell lines. HCT116, colo320DM, SW837, HT-29 were maintained in RPMI medium (Sigma, St. Louis, MO) with 10% fetal bovine serum (FBS) (Sigma) and penicillin/streptomycin (GIBCO, Rockville, MD). Human umbilical vein endothelial cells (HUVECs) were maintained in HuMedia EG2 (Kurabo, Osaka, Japan).

Western blotting. Total cell lysates were heated for 3 min at 95 °C and then loaded onto SDS–polyacrylamide gels. Proteins were electrophoretically transferred onto polyvinylidene difluoride membranes (Millipore, MA, USA), blocked with 5% nonfat dry milk, then blotted with anti-PSF3 antibody or anti-beta actin antibody (Sigma). Blots were developed with peroxidase-labeled anti-mouse Ig antibodies (Dako, Carpinteria, CA) using enhanced chemiluminescence (ECL detection system; Amersham, Buckinghamshire, UK).

Immunocytochemistry. For staining of PSF1 and PSF3, 4% PFA in phosphate buffer saline (PBS) and cold methanol was used for fixations. Following three washes with PBS, cells were incubated with anti-PSF1 [15] and anti-PSF3 antibody, then washed with PBS and incubated with goat anti-mouse IgG Alexa488 (for PSF3, Invitrogen, Carlsbad, CA, USA) or anti-rat IgG Biotin (for PSF1, Invitrogen) followed by Streptavidin-Cy3 (Zymed). Nuclear DNA was counter-stained with Hoechst (Sigma).

Immunohistochemistry. For human specimens, immnohistochemistry was performed on formalin-fixed, paraffin-embedded tumor samples. All specimens were obtained from the Department of Gastroenterological Surgery, Graduate School of Medicine, Osaka University. For the immunohistochemical analyses, mouse anti-PSF3 antibody (aps3.2) or anti-Ki-67 antibody (Dako) was used for primary antibodies. As a secondary antibody for anti-PSF3 or anti-Ki-67 antibody, Biotin-conjugated goat anti-mouse Ig (Dako) was used. After washing the slides three times with 0.05% Triton X-100 in PBS, they are incubated with VECSTAIN ABC Standard

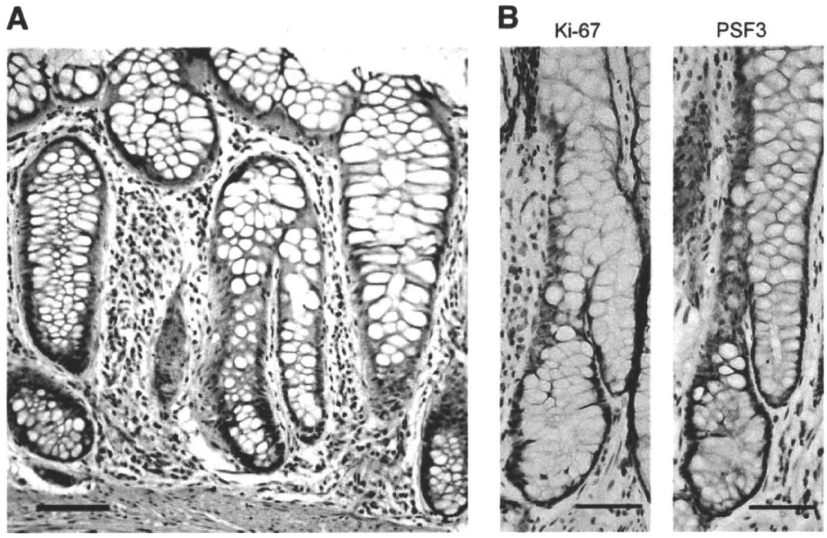

Fig. 2. PSF3 expression in human colonic mucosa. (A) Immunohistochemical analysis of PSF3 (brown) expression in human colonic mucosa. Bar, 100 μm. (B) Immunohistochemical analysis of Ki-67 (brown) and PSF3 (brown) expression in serial sections of human colon mucosa. Bars, 50 μm.

Kit (Vector Laboratories, Burlingame, CA, USA). For the visualization of HRP, diaminobenzidine (Dojindo, Kumamoto, Japan) was used. The slides were counter-stained with hematoxylin.

RNA interference. Small interfering RNA (siRNA) specific to human PSF3 and negative control siRNA were purchased from Invitrogen. The effect of siRNA transfection was optimized using RNAiMAX (Invitrogen) according to the manufacturer's protocol. The effect of siRNA on PSF3 expression was observed using Western blotting with an anti-PSF3 antibody. Cell numbers were counted by a hemocytometer.

BrdU-FACS. For BrdU detection, 10 μM BrdU was added to the medium for 15 min prior to cell collection. Cells were fixed in 70% ethanol and washed in PBS, treated with 1 N HCl for 30 min and incubated with anti-BrdU antibody (BD Bioscience Pharmingen, SanDiego, USA), followed by anti-mouse IgG Alexa488 (Invitrogen).

Results

PSF3 expression in human colon carcinoma cell lines

We compared the expression of PSF3 in human colon carcinoma cell lines and non-tumor cells (HUVECs). Overall, tumor cells expressed higher levels of PSF3 protein than HUVECs (Fig. 1A and B). Next, we performed immunocytochemistry to localize PSF3 in colon carcinoma cells. Nuclear accumulation of PSF3 was observed during interphase, whereas during mitosis, it was almost exclusively located outside the chromatin with a diffuse pattern

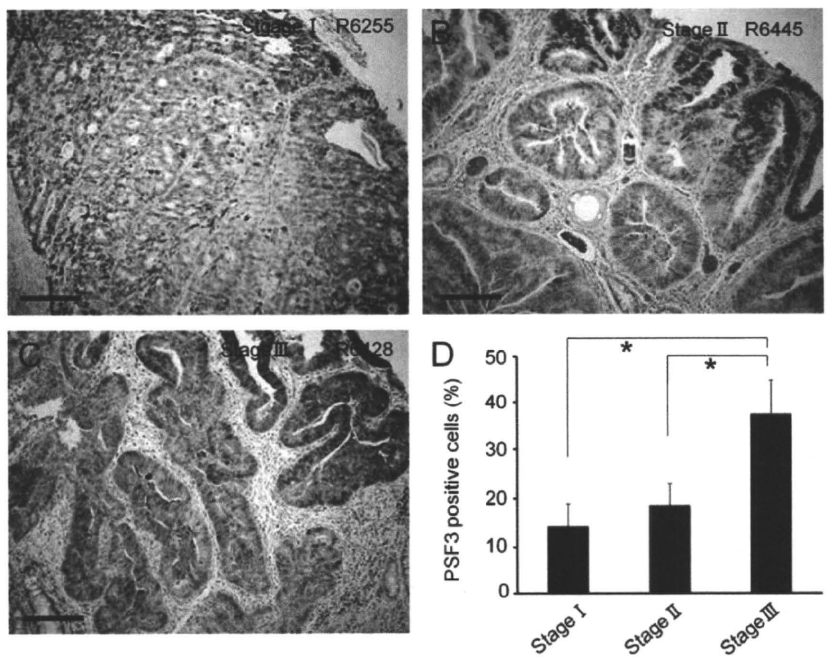

Fig. 3. PSF3 expression in human colon carcinoma specimens. (A–C) PSF3 (brown) expression in human colon carcinoma specimens in different stages (A, stage I; B, stage II; C, stage III). Bars, 200 μm. (D) Percentages of tumor cells that are PSF3-positive. *$P < 0.05$ ($n = 6$, mean ± SEM).

(Fig. 1C). These characteristics are similar to PSF1, one of the other GINS components (Fig. 1C), suggesting colocalization of PSF3 and PSF1 as a GINS component in human colon carcinoma cells.

PSF3 expression in human normal colonic mucosa and colon carcinoma specimens

Several studies have suggested that GINS components play a role in tumor progression [16–18]. To test whether PSF3 may also be involved in human colon cancer progression, its expression in colon carcinoma pathological specimens was investigated using immunohistochemistry.

In adjacent normal large bowel mucosa, PSF3 expression was confined to the base of the colon crypts, which corresponds to the proliferative zone of the mucosa (Fig. 2A). Using serial tissue sections, we compared expression of PSF3 with Ki-67, a marker of proliferation. The majority of PSF3-positive cells was found to co-express Ki-67 (Fig. 2B), indicating cell cycling. Our previous study showed that PSF1 is also expressed in crypt base columnar cells and that the number of such cells decreased in adult haploinsufficient *PSF1*$^{+/-}$ mice compared with adult wild-type mice [15]. Based on these results, we suggest that the GINS complex may play an important role in proliferation of colon crypt cells.

Additionally, in colon carcinoma specimens from patients, higher levels of expression of PSF3 protein were found in the cancer cells than the adjacent normal mucosa. Moreover, the percentage of PSF3-positive cancer cells correlated positively with the stage of cancer (Fig. 3). This further suggests that PSF3 protein expression associates with colon cancer progression.

PSF3 knock-down results in growth arrest of human colon carcinoma cells

To assess whether PSF3 is involved in colon cancer cell proliferation, we evaluated the silencing effect of PSF3 on cell growth using RNAi methodology to target three different coding regions of the human *PSF3* mRNA sequence. The efficiency of *PSF3* knock-down was examined by Western blotting, indicating that PSF3 protein expression in both HCT116 and colo320DM cells was greatly attenuated, in particular by two different sequences (siPSF3-2, 3) (Fig. 4A). PSF3 knock-down in either cell line resulted in inhibition of proliferation (Fig. 4B). This inhibitory effect correlated with PSF3 expression silencing efficiency, because less effects on cell proliferation were observed with siPSF3-1. The relationship of cell cycling to reduction of PSF3 expression was assessed by the incorporation of nucleotide analogues. Results indicated that attenuation of PSF3

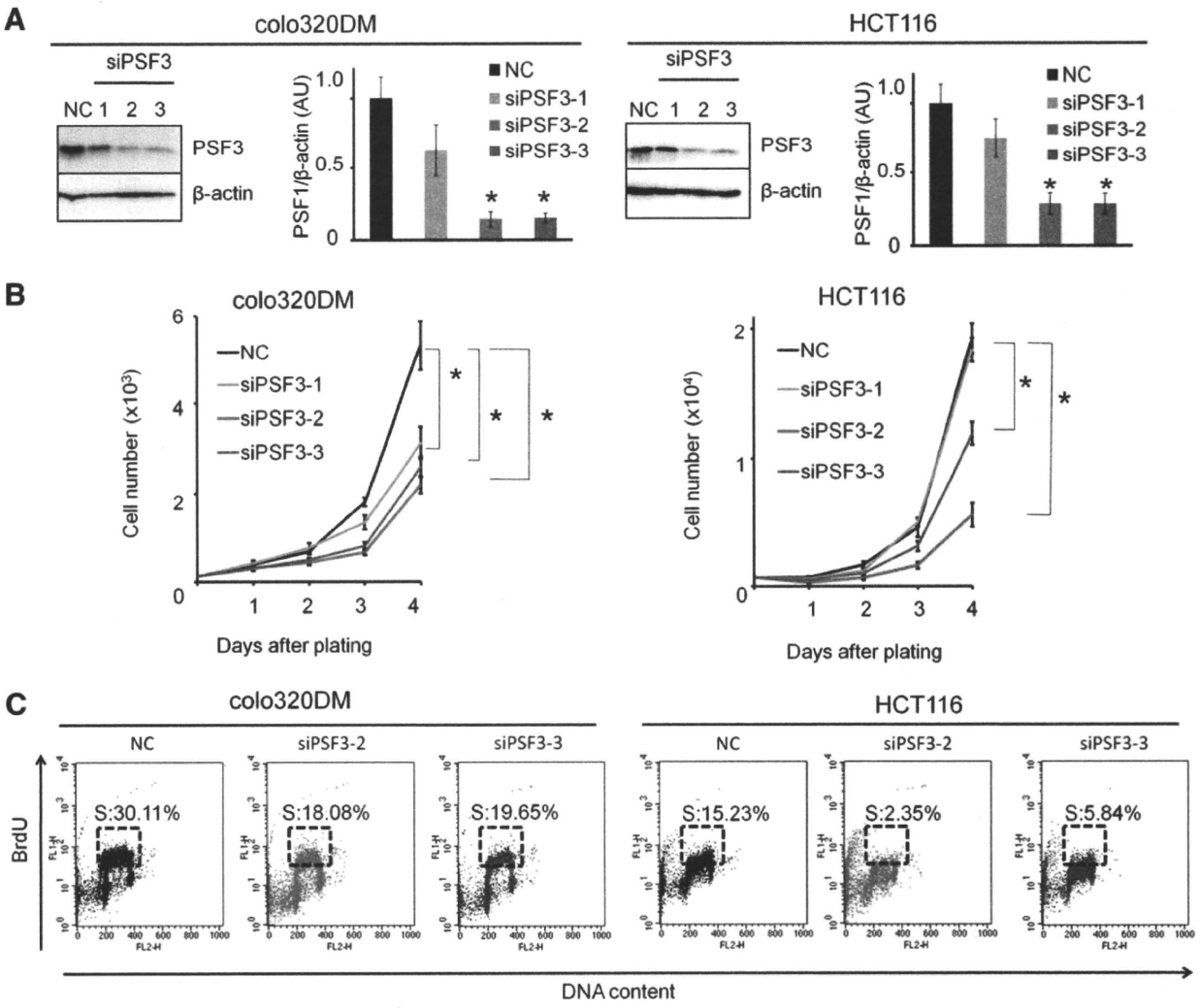

Fig. 4. PSF3 knock-down results in growth inhibition in colon carcinoma cell lines. (A) Western blotting for PSF3 expression after silencing by three RNAis (siPSF3-1, 2 and 3) or a control RNAi (NC). Densitometric analysis was performed for quantitative evaluation ($n = 4$). *$P < 0.05$ vs control. (B) Cell growth after introduction of RNAi as described in (A). *$P < 0.05$ ($n = 8$, mean ± SEM). (C) Cellular BrdU incorporation assay was carried out 48 h after transfection with the indicated siRNA. BrdU was incorporated for 15 min. BrdU intensity is represented in the logarithmic y-axis and DNA content on the linear x-axis. Gates define the percentage of cells in S-phase.

expression reduced the percentage of cells in S-phase (Fig. 4C). Thus, we conclude that PSF3 plays a role in cell cycling, especially S-phase progression.

Discussion

In this study, we found high levels of expression of PSF3 in several colon carcinoma cell lines and overexpression of PSF3 in stage-matched human colon cancer cells from higher grade tumors. Our preliminary experiments showed that PSF3 is more highly expressed in cancer cells invading into muscle than in non-invasive cancer (data not shown). It has been reported that several prereplicative complex proteins are overexpressed in cancer and serve as good tumor markers [19]. For example, MCM-2 (a member of the C–M–G complex) was reported to be significantly associated with Dukes' stage, existence of lymph node metastasis, tumor histological grade, presence of malignancy in adenoma, and venous invasion in colon cancer [20]. Based on these findings, our present data suggest that PSF3 might be a potential biomarker for diagnosis of progression and during the initiation of metastasis in colon cancer. Comparison of PSF3 with other proliferation markers, such as Ki-67 and PCNA, might support this hypothesis.

Previous studies have shown that DNA replication factors, including GINS, are differently expressed in *Xenopus*, suggesting that different factors are utilized in different developmental regions [21]. Further studies of precise expression profiles and functions of individual GINS components in mammalian tissues might help us to understand how such individual components are involved in tumor growth occurring in a wide variety of tissues and organs. Here, we documented PSF3 expression in the base of the crypts in normal colon and found that PSF3 expression was co-localized with PSF1 in human colon carcinoma cell lines. Moreover, PSF3 knock-down resulted in growth inhibition of colon cancer cells by the suppression of S-phase progression, indicating that PSF3 acts at least as a GINS complex and is essential for S-phase progression in human colon carcinoma cells. Further studies are required to elucidate the contributions of individual GINS components in the growth of other tumors.

Several studies have indicated that pre-RC proteins may potentially have significant therapeutic value [19]. Interestingly, Orc6, one such pre-RC protein, was reported to be associated with 5-fluorouracil (5-FU) resistance in human colon cancer cell lines [22], and its downregulation sensitized colon cancer cells to 5-FU and cisplatin [23]. These results suggest that pre-RC proteins may play a role in chemoresistance. Based on these reports, our data suggest that PSF3 might be a potential therapeutic target as well as a potential diagnosis marker for colon carcinoma.

Acknowledgments

We are grateful to N. Fujimoto and K. Fukuhara for technical assistance. This work was partly supported by the Japanese Ministry of Education, Culture, Sports, Science and Technology and the Japanese Society for Promotion of Science.

References

[1] Y. Takayama, Y. Kamimura, M. Okawa, S. Muramatsu, A. Sugino, H. Araki, GINS, a novel multiprotein complex required for chromosomal DNA replication in budding yeast, Genes Dev. 17 (2003) 1153–1165.
[2] C. Bauerschmidt, S. Pollok, E. Kremmer, H.P. Nasheuer, F. Grosse, Interactions of human Cdc45 with the Mcm2–7 complex, the GINS complex, and DNA polymerases delta and epsilon during S phase, Genes Cells 12 (2007) 745–758.
[3] A. Gambus, R.C. Jones, A. Sanchez-Diaz, et al., GINS maintains association of Cdc45 with MCM in replisome progression complexes at eukaryotic DNA replication forks, Nat. Cell Biol. 8 (2006) 358–366.
[4] M. Kanemaki, A. Sanchez-Diaz, A. Gambus, K. Labib, Functional proteomic identification of DNA replication proteins by induced proteolysis in vivo, Nature 423 (2003) 720–724.
[5] S.E. Moyer, P.W. Lewis, M.R. Botchan, Isolation of the Cdc45/Mcm2–7/GINS (CMG) complex, a candidate for the eukaryotic DNA replication fork helicase, Proc. Natl. Acad. Sci. USA 103 (2006) 10236–10241.
[6] M. Pacek, A.V. Tutter, Y. Kubota, H. Takisawa, J.C. Walter, Localization of MCM2–7, Cdc45, and GINS to the site of DNA unwinding during eukaryotic DNA replication, Mol. Cell 21 (2006) 581–587.
[7] Y.P. Chang, G. Wang, V. Bermudez, J. Hurwitz, X.S. Chen, Crystal structure of the GINS complex and functional insights into its role in DNA replication, Proc. Natl. Acad. Sci. USA 104 (2007) 12685–12690.
[8] M. De Falco, E. Ferrari, M. De Felice, M. Rossi, U. Hubscher, F.M. Pisani, The human GINS complex binds to and specifically stimulates human DNA polymerase alpha-primase, EMBO Rep. 8 (2007) 99–103.
[9] K. Kamada, Y. Kubota, T. Arata, Y. Shindo, F. Hanaoka, Structure of the human GINS complex and its assembly and functional interface in replication initiation, Nat. Struct. Mol. Biol. 14 (2007) 388–396.
[10] Y. Kubota, Y. Takase, Y. Komori, et al., A novel ring-like complex of *Xenopus* proteins essential for the initiation of DNA replication, Genes Dev. 17 (2003) 1141–1152.
[11] L.R. Barkley, I.Y. Song, Y. Zou, C. Vaziri, Reduced expression of GINS complex members induces hallmarks of pre-malignancy in primary untransformed human cells, Cell Cycle 8 (2009) 1577–1588.
[12] A.S. Hemerly, S.G. Prasanth, K. Siddiqui, B. Stillman, Orc1 controls centriole and centrosome copy number in human cells, Science 323 (2009) 789–793.
[13] M. Ueno, M. Itoh, L. Kong, K. Sugihara, M. Asano, N. Takakura, PSF1 is essential for early embryogenesis in mice, Mol. Cell. Biol. 25 (2005) 10528–10532.
[14] Y. Han, M. Ueno, Y. Nagahama, N. Takakura, Identification and characterization of stem cell-specific transcription of PSF1 in spermatogenesis, Biochem. Biophys. Res. Commun. 380 (2009) 609–613.
[15] M. Ueno, M. Itoh, K. Sugihara, M. Asano, N. Takakura, Both alleles of PSF1 are required for maintenance of pool size of immature hematopoietic cells and acute bone marrow regeneration, Blood 113 (2009) 555–562.
[16] K. Obama, K. Ura, S. Satoh, Y. Nakamura, Y. Furukawa, Up-regulation of PSF2, a member of the GINS multiprotein complex, in intrahepatic cholangiocarcinoma, Oncol. Rep. 14 (2005) 701–706.
[17] R. Hayashi, T. Arauchi, M. Tategu, Y. Goto, K. Yoshida, A combined computational and experimental study on the structure–regulation relationships of putative mammalian DNA replication initiator GINS, Genomics Proteomics Bioinformatics 4 (2006) 156–164.
[18] B. Ryu, D.S. Kim, A.M. Deluca, R.M. Alani, Comprehensive expression profiling of tumor cell lines identifies molecular signatures of melanoma progression, PLoS One 2 (2007) e594.
[19] E. Lau, T. Tsuji, L. Guo, S.H. Lu, W. Jiang, The role of pre-replicative complex (pre-RC) components in oncogenesis, FASEB J. 21 (2007) 3786–3794.
[20] C. Giaginis, M. Georgiadou, K. Dimakopoulou, et al., Clinical significance of MCM-2 and MCM-5 expression in colon cancer: association with clinicopathological parameters and tumor proliferative capacity, Dig. Dis. Sci. 54 (2009) 282–291.
[21] B.E. Walter, J.J. Henry, Embryonic expression of pre-initiation DNA replication factors in *Xenopus laevis*, Gene Expr. Patterns 5 (2004) 81–89.
[22] Y. Xi, G. Nakajima, J.C. Schmitz, E. Chu, J. Ju, Multi-level gene expression profiles affected by thymidylate synthase and 5-fluorouracil in colon cancer, BMC Genomics 7 (2006) 68.
[23] E.J. Gavin, B. Song, Y. Wang, Y. Xi, J. Ju, Reduction of Orc6 expression sensitizes human colon cancer cells to 5-fluorouracil and cisplatin, PLoS One 3 (2008) e4054.

Published OnlineFirst January 26, 2010; DOI:10.1158/0008-5472.CAN-09-3662

AACR

Cancer Research

PSF1, a DNA Replication Factor Expressed Widely in Stem and Progenitor Cells, Drives Tumorigenic and Metastatic Properties

Yumi Nagahama, Masaya Ueno, Satoru Miyamoto, et al.

Cancer Res 2010;70:1215-1224. Published OnlineFirst January 26, 2010.

Published OnlineFirst January 26, 2010; DOI:10.1158/0008-5472.CAN-09-3662

Tumor and Stem Cell Biology

Cancer Research

PSF1, a DNA Replication Factor Expressed Widely in Stem and Progenitor Cells, Drives Tumorigenic and Metastatic Properties

Yumi Nagahama[1], Masaya Ueno[1], Satoru Miyamoto[1], Eiichi Morii[2], Takashi Minami[4], Naoki Mochizuki[3], Hideyuki Saya[5], and Nobuyuki Takakura[1]

Abstract

PSF1 (partner of sld five 1) is an evolutionarily conserved DNA replication factor implicated in DNA replication in lower species that is strongly expressed in a wide range of normal stem cell populations and progenitor cell populations. Because stem and progenitor cells possess high proliferative capacity, we hypothesized that PSF1 may play an important role in tumor growth. To begin to investigate PSF1 function in cancer cells, we cloned the mouse PSF1 promoter and generated lung and colon carcinoma cells that stably express a PSF1 promoter-reporter gene. Reporter expression in cells correlated with endogenous PSF1 mRNA expression. In a tumor cell xenograft model, high levels of reporter expression correlated with high proliferative activity, serial transplantation potential, and metastatic capability. Notably, cancer cells expressing reporter levels localized to perivascular regions in tumors and displayed expression signatures related to embryonic stem cells. RNAi-mediated silencing of endogenous PSF1 inhibited cancer cell growth by disrupting DNA synthesis and chromosomal segregation. These findings implicate PSF1 in tumorigenesis and offer initial evidence of its potential as a theranostic target. *Cancer Res; 70(3); 1215–24. ©2010 AACR.*

Introduction

PSF1 (partner of SLD5) is a member of the tetrameric complex termed GINS, composed of SLD5, PSF1, PSF2, and PSF3, and is well conserved evolutionarily. In yeast, the GINS complex associates with the MCM2-7 complex and CDC45, and this "C-M-G complex" (CDC45-MCM2-7-GINS) regulates both the initiation and the progression of DNA replication (1–6). In *Xenopus* and human, GINS has been suggested to be involved in DNA replication because of its binding to DNA replication protein (7–10); however, a recent study suggests that PSF1/2 is associated with the response to replication stress and acquisition of DNA damage in untransformed human dermal fibroblasts (11). Thus, the exact functions of GINS components in mammalian cells are not yet clear.

Authors' Affiliations: [1]Department of Signal Transduction, Research Institute for Microbial Diseases, Osaka University; [2]Department of Pathology, Osaka University School of Medicine; [3]Department of Structural Analysis, National Cardiovascular Center Research Institute, Suita, Osaka, Japan; [4]Laboratory for Systems Biology and Medicine, Research Center for Advanced Science and Technology (LSBM), University of Tokyo, Meguro, Tokyo, Japan; and [5]Division of Gene Regulation, Institute for Advanced Medical Research, Keio University School of Medicine, Shinjyuku-ku, Tokyo, Japan

Note: Supplementary data for this article are available at Cancer Research Online (http://cancerres.aacrjournals.org/).

Corresponding Author: Nobuyuki Takakura, Department of Signal Transduction, Research Institute for Microbial Diseases, Osaka University, 3-1 Yamada-oka, Suita, Osaka 565-0871, Japan. Phone: 81-6-6879-8312; Fax: 81-6-6879-8314; E-mail: ntakaku@biken.osaka-u.ac.jp.

doi: 10.1158/0008-5472.CAN-09-3662

We have previously cloned the mouse ortholog of *PSF1* from a hematopoietic stem cell cDNA library (12) and found that PSF1 expression in mice was predominantly observed in the adult bone marrow and thymus, as well as the testis and ovary (i.e., tissues in which stem cell proliferation is actively induced and continues after birth). Moreover, we reported that PSF1 is strongly expressed in different immature cell lineages, such as cells in the inner cell mass during early embryogenesis as well as spermatogonia and hematopoietic stem cells after birth (12–14). Loss of PSF1 led to embryonic lethality around the implantation stage caused by the inability of cells of the inner cell mass to proliferate (12). Moreover, haploinsufficiency of PSF1 in $PSF1^{+/-}$ mice resulted in the delayed induction of hematopoietic stem cell proliferation during reconstitution of bone marrow after 5-fluorouracil ablation. These data strongly suggest that PSF1 is required for acute proliferation of cells, especially immature cells such as stem cells and progenitor cells.

Several recent studies have suggested that GINS components play a role not only in immature cells from normal tissues, as we reported, but also in cancer cells. For example, all GINS components were found to be overexpressed in intrahepatic cholangiocarcinoma tissues (15). A Gene Expression Omnibus (GEO) database search revealed that *PSF1* is an estrogen target in MCF7 human breast carcinoma cells (16). In a comprehensive study, it was found that *PSF1* and *SLD5* were upregulated in aggressive melanoma (17). Based on these results, we examined the nature of cells highly expressing PSF1 in a tumor xenograft model.

Genetic events caused by epigenetic modulation and microenvironmental exposure have been suggested to be responsible

Published OnlineFirst January 26, 2010; DOI:10.1158/0008-5472.CAN-09-3662

for tumor progression. Therefore, a species-matched (murine) microenvironment is needed to examine the nature of cells strongly expressing PSF1.

Here, we have investigated the expression of PSF1 and the localization of PSF1-positive cancer cells in a mouse tumor cell xenograft model. We observed malignant behavior of highly PSF1-positive tumor cells with regard to tumorigenesis and metastasis. Moreover, highly PSF1-positive cancer cells have been characterized by microarray analysis, and the data compared with those of the recently reported embryonic stem cell (ESC)–like gene expression signature in poorly differentiated aggressive human tumors (18). Finally, to determine whether PSF1 could be a molecular target for the development of anticancer drugs, we silenced the *PSF1* gene by the RNA interference (RNAi) method in human carcinoma cell lines and observed the effects thereof on the growth of the cancer cells.

Materials and Methods

Cell culture and cell line construction. LLC, B16, NIH3T3, HeLa, and HEK293T were maintained in DMEM (Sigma) with 10% fetal bovine serum (FBS; Sigma) and penicillin/streptomycin (Life Technologies, Inc.). Colon26 cells were maintained in RPMI 1640 (Sigma) with 10% FBS and penicillin/streptomycin. Mouse embryonic fibroblasts were prepared from day 14.5 embryos and cultured in high-glucose DMEM (Sigma) with 10% FBS and penicillin/streptomycin.

The gene encoding the PSF1 promoter region was isolated by mouse BAC cloning (RP23-193L22, Advanced GenoTechs Co.). Using the 5′ upstream sequence of the first exon of the *PSF1* locus as a probe, 5.5 kb of the 5′flanking PSF1 gene were isolated and subcloned into pBluescript II KS (Stratagene). The enhanced green fluorescent protein (*EGFP*) gene and the *neomycin* gene were excised from pEGFP-N1 and pcDNA3.1(−) (Clontech), respectively, and ligated to the 5.5 kb of the PSF1 5′-flanking fragment. This construct was designated *PSF1p-EGFP*. LLC and colon26 cells were transfected using Lipofectamine 2000 (Invitrogen). After transfection, the cells were cultured in medium supplemented with G418 (Life Technologies) to obtain cells stably expressing EGFP under the control of the PSF1 promoter (LLC-*PSF1p-EGFP* and colon26-*PSF1p-EGFP*).

Quantitative reverse transcription-PCR. Quantitative reverse transcription-PCR (RT-PCR) was done as previously described (14). The primer sets were described in Supplementary Materials and Methods.

Mice. Seven- to eight-week-old C57BL/6 female mice (for the LLC experiments) and BALB/c female mice of the same age (for colon26) were purchased from Japan SLC. All animal studies were approved by the Osaka University Animal Care and Use Committee. Subcutaneous xenografts were established by injecting 10^6 cells into the flanks of the mice.

Flow cytometric analysis. Single-cell suspensions from tumors were prepared using a standard protocol. Cell sorting was done using a FACSAria (Becton Dickinson). For the EGFP^{high} population, the 5% most brightly fluorescing cells were sorted, and for the EGFP^{low} population, the 5% least fluorescent. We used parental LLC or colon26 as negative controls.

In vitro *clonal analyses and* in vivo *tumorigenicity analysis.* Isolated cells were plated on 10-cm culture dishes (200 per dish for LLC-*PSF1p-EGFP* and 100 per dish for colon26-*PSF1p-EGFP*) and cultured. The percentage of cells that initiated a clone was taken as the plating efficiency. For *in vivo* experiments, 100 sorted cells in 100 μL of PBS with growth factor–reduced Matrigel (BD Biosciences; 1:1) were injected s.c. into the mice. Five weeks after injection, tumor volumes were measured with a caliper and calculated as width × width × length × 0.52.

Invasion assay and metastasis assay. The invasive activity of tumor cells was assayed using a BioCoat Matrigel Invasion Chamber (BD Biosciences) according to the manufacturer's instruction.

For the lung metastasis assay using LLC-*PSF1p-EGFP*, 10^5 viable sorted cells were injected into the tail veins of mice. After 4 wk, lungs were dissected and the number of colonies observable on the surface of the lungs was noted. For the hepatic metastasis assay of colon26-*PSF1p-EGFP*, spleens of mice were exposed to allow the direct injection of 5×10^4 viable sorted cells. After 12 d, livers and spleens were dissected out and the number of colonies observable on the surface of the livers was recorded. Sections of liver were stained with H&E to evaluate tissue morphology and to detect metastases.

Immunohistochemistry and immunocytochemistry. Immunohistochemical analyses were done as previously described (19). Rabbit anti-GFP antibody (Invitrogen) and rat anti-CD31 (BD Biosciences) were used for primary antibodies. For the fluorescent immunohistochemical analyses, phycoerythrin-conjugated anti-CD31 (BD Biosciences) was used for staining endothelial cells.

For immunocytochemistry, anti-PSF1(14), anti-bromodeoxyuridine (BrdUrd) (Zymed Laboratories), anti–β-tubulin (Sigma), anti–CENP-A (MBL), and anti-survivin (Chemicon International, Inc.) antibodies were used as previously described (14).

PSF1 *knockdown.* Transfection was done using Lipofectamine 2000 (Invitrogen). For the enrichment of transiently shRNA vector–transfected cells, the puromycin resistance gene was ligated into the *Xho*I site of the pSINsi-hU6 vector (Takara), and then sense and antisense oligonucleotide pairs (see below) were annealed and ligated into the *Bam*HI/*Cla*I site of the pSINsi-hU6-P vectors. The sequences of the oligonucleotide sets were described in Supplementary Materials and Methods. For time-lapse imaging of histone H3 and tubulin in living cells, HEK293T cells were transfected with GFP-histone (20) or tubulin-GFP (Clontech) expression vectors, and stably expressing clones were selected. Time-lapse observation was done as previously reported using an IX70 microscope (Olympus; ref. 21).

Microarray and bioinformatics analysis. Microarrays were done as previously described (22). Raw data are available for download from GEO (GSE17112). Gene set enrichment analysis (GSEA; ref. 23) was done by CeresBioscience as previously reported.

Statistical analysis. Results were expressed as the mean ± SEM. Student's *t* test was used for statistical analysis. Differences were considered statistically significant when $P < 0.01$.

Published OnlineFirst January 26, 2010; DOI:10.1158/0008-5472.CAN-09-3662

Results

Establishment of transgenic cell lines to monitor endogenous* PSF1 *expression in living cells. We first examined *PSF1* mRNA expression in mouse cancer cell lines, a noncancer cell line, and primary cultured cells. *PSF1* mRNA in cancer cell lines is expressed to a greater degree than in the noncancer cell line or primary cultured cells (Fig. 1A). To determine whether the cancer cells strongly expressing PSF1 had malignant features, they need to be collected as living cells. Because PSF1 is an intracellular protein, viable cells cannot be isolated using PSF1 antibody and flow cytometric cell sorting. Therefore, we used promoter activity to monitor the expression level of PSF1 in cancer cells in the murine tumor xenograft model. We have cloned the mouse *PSF1* promoter gene and established lung carcinoma [Lewis lung carcinoma (LLC)] and colon cancer (colon26) cell lines stably expressing EGFP under the transcriptional control of the *PSF1* promoter (LLC- and colon26-*PSF1p-EGFP*, respectively). We confirmed *PSF1* mRNA expression in parental LLC and colon26 cells (data not shown). After inoculation of LLC-*PSF1p*-EGFP, tumors were dissected and the intensity of EGFP in dissociated cancer cells was analyzed by flow cytometry (Fig. 1B–D). As can be seen, EGFP-positive ($EGFP^+$) cells containing high or low levels of EGFP ($EGFP^{high}$ or $EGFP^{low}$ cells, respectively) were present. These were separated and the expression of *PSF1* mRNA was examined (Fig. 1D). The results indicate that the intensity of EGFP is correlated with the endogenous *PSF1* expression. Similar results were obtained using colon26-*PSF1p-EGFP* (data not shown). These results suggest that these cell lines are useful tools to monitor endogenous *PSF1* expression in living cells.

EGFP(PSF1)^{high} cells possess greater tumorigenic capacity. To study their colony forming efficiency, cancer cells

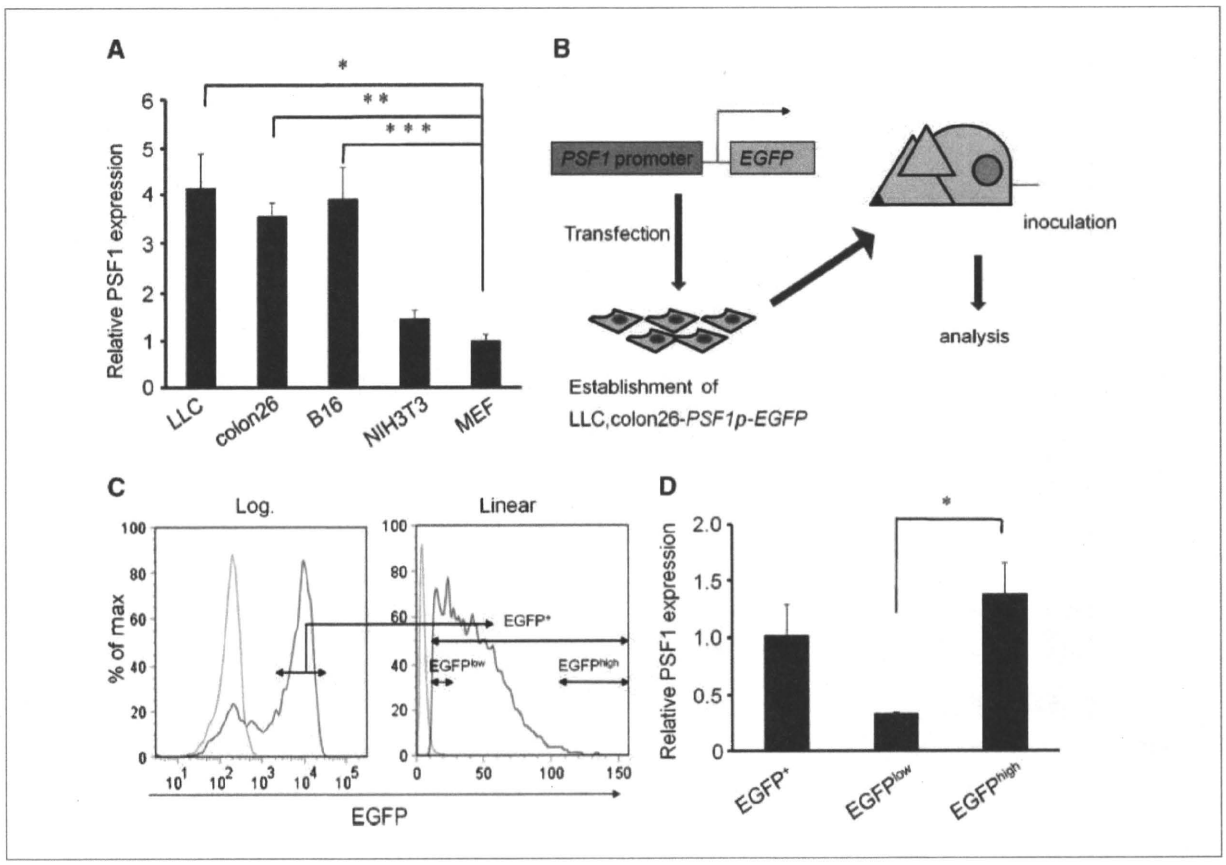

Figure 1. PSF1 expression in murine carcinoma cell lines. A, expression of *PSF1* mRNA in murine carcinoma cells. Total RNA was analyzed by quantitative RT-PCR for *PSF1* expression in different murine carcinoma cell lines and compared with a noncancer cell line and a primary cell culture. The values are normalized to the amount of mRNA in mouse embryonic fibroblasts. *LLC*, lung carcinoma; *colon26*, colon carcinoma; *B16*, melanoma; *NIH3T3*, mouse embryonic fibroblast cell line; *MEF*, mouse embryonic fibroblast. Data show the mean ± SEM. *, **, ***, $P < 0.01$ ($n = 3$). B, experimental procedure. We have cloned the mouse *PSF1* promoter gene and established cell lines stably expressing EGFP under the transcriptional control of the *PSF1* promoter (LLC- and colon26-*PSF1p-EGFP*, respectively). After inoculation of LLC- or colon26-*PSF1p*-EGFP, tumors were dissected and the dissociated cancer cells were separated using a cell sorter according to the intensity of EGFP expression and further analyzed. C, fluorescence-activated cell sorting analysis of cells from tumor tissues injected with LLC (green) or LLC-*PSF1p-EGFP* (red) cells. $EGFP^+$, $EGFP^{low}$, and $EGFP^{high}$ cells were sorted as indicated. Intensity of EGFP is displayed on a log or linear scale. D, quantitative RT-PCR analysis of *PSF1* mRNA expression in sorted cells as indicated. The values are normalized to the amount of mRNA in $EGFP^+$ cells. Data show the mean ± SEM. *, $P < 0.01$ ($n = 3$).

Published OnlineFirst January 26, 2010; DOI:10.1158/0008-5472.CAN-09-3662

(LLC- and colon26-*PSF1p-EGFP*) from tumor-bearing mice were divided into three fractions (EGFP$^+$, EGFP^{low}, and EGFP^{high}) as indicated in Fig. 1C, seeded, and cultured for 2 weeks. EGFP^{high} cells formed significantly larger colonies than did EGFP^{low} cells (Fig. 2A) in both colon26 and LLC tumors.

We next examined the serial transplantation ability of these cells. We inoculated sorted EGFP^{high} or EGFP^{low} cells from tumor-bearing mice into new hosts to evaluate the relationship between PSF1 expression and tumorigenicity. Four weeks (LLC-*PSF1p-EGFP*) or 2 weeks (colon26-*PSF1p-EGFP*) after initial inoculation, 100 sorted EGFP$^+$, EGFP^{low}, or EGFP^{high} tumor cells were again transplanted into new hosts. EGFP^{high} cells from both LLC and colon26 tumors formed significantly larger tumors than did EGFP^{low} or EGFP$^+$ cells (Fig. 2B). When tumor cell components were examined in tumors generated after the second transplantation, EGFP^{high} cells were found to have given rise to both EGFP^{high} and EGFP^{low} cells in both LLC and colon26 tumors (Supplementary Fig. S1). Taken together, these data suggest that cancer cells expressing higher levels of *PSF1* exhibit high cloning efficiency and tumorigenicity.

EGFP(PSF1)^{high} cells possess greater invasive and metastatic capacity. We investigated that EGFP^{high} cells also play a crucial role in tumor metastasis. We determined the overall ability of cells sorted, as described in Fig. 1C, for invasion using Matrigel, a basement membrane model used to estimate metastatic potential. EGFP^{high} cells migrated more effectively than did EGFP^{low} cells or EGFP$^+$ cells, indicating that they possess greater invasive capacity (Fig. 3A and B).

Next, we examined the *in vivo* metastatic potential of these cells by two different means. First, viable sorted EGFP^{high} or EGFP^{low} cells from LLC tumors were injected into the tail veins of recipient mice. After 4 weeks, macrometastatic lesions

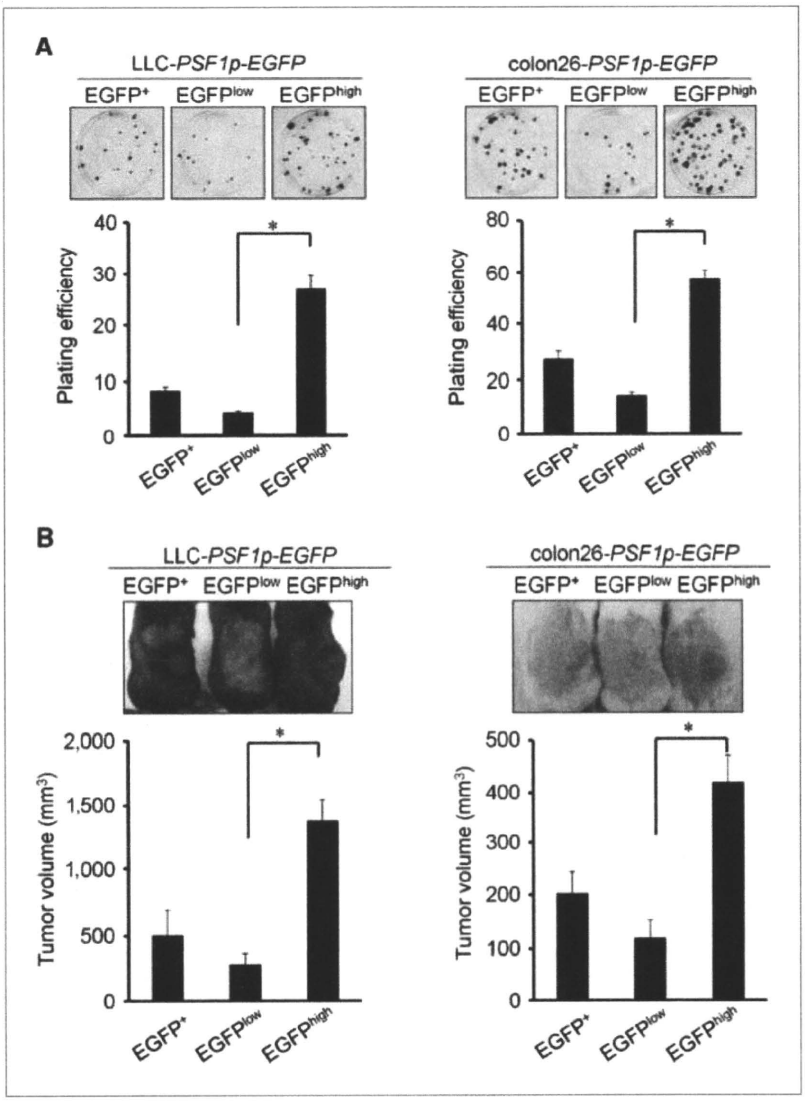

Figure 2. High proliferative ability of PSF1^{high} cancer cells. A, plating efficiency of sorted cells. Sorted cells from tumor tissues injected with LLC-*PSF1p-EGFP* or colon26-*PSF1p-EGFP* were seeded onto 10-cm culture dishes and cultured for 2 wks. Colonies generated from different fractions as indicated were stained with Giemsa solution (top). Quantitative evaluation of colonies from each fraction as indicated. Percentages of the colony numbers relative to the number of cells seeded are presented (bottom). Data show the mean ± SEM. *, $P < 0.01$ ($n = 3$). Results shown are representative of at least three independent experiments. B, tumorigenesis assay. Gross appearance of the tumor mass in mice 5 wks after inoculation with sorted cancer cells as indicated (top). Tumor volume was determined 5 wks after inoculation with sorted cells as indicated (bottom). Data show the mean ± SEM. *, $P < 0.01$ ($n = 10$). Experiments were done at least three times with similar results.